Harmonic Radar With Adaptively Phase-Coherent Auxiliary Transmitters

Anastasia Lavrenko, *Member, IEEE*, James K. Cavers, *Life Fellow, IEEE*, and Graeme K. Woodward, *Senior Member, IEEE*

***Abstract*—In harmonic radar (HR), the transmitter illuminates a nonlinear target (the tag), causing the return signal to consist of harmonics at multiples of the transmitted carrier frequency. Of them, the second harmonic is usually the strongest and the one to which the receiver is tuned. This frequency difference distinguishes the tag reflection from environmental clutter, which remains at the illuminating frequency. However, the passive nature of HR tags severely limits the reflected power, and therefore the operational range of a HR system. We propose to increase the range and/or signal to noise ratio (SNR) by novel restructuring at the physical and signal levels. For this, we accompany the original transmitter with auxiliary transmitters able to send simple tones that are synchronized to arrive at the tag in phase, and we design the receiver to detect an intermodulation component. The resulting range and SNR are much greater than those of the original, conventional HR system, even if the original system were to transmit with power equal to the aggregate power of the proposed system. Achieving mutually coherent, (in phase), arrival of the tones at the tag is the focus of the present paper. We provide a system framework that models the tag, then present the adaptive phase coherence algorithm and analyze the probabilistic growth of the output signal power. We also account for the effects of frequency shifts due to transmitter mobility and the frequency offset errors in the transmitter local oscillators.**

***Index Terms*—Harmonic radar, harmonic tags, harmonic RFID, nonlinear radar, auxiliary transmitters, adaptive phase coherence, range extension.**

I. Introduction

HARMONIC radar (HR) is the basis of many schemes that interrogate, or track the location of, a simple nonlinear tag [1]–[5]. Tracking of insect movement [6] and discovery of nonlinear electronic circuitry [7] are typical applications. HR-based interrogation schemes have also recently been used for designing harmonic RFID systems in a variety of IoT applications [8], [9]. Common examples include temperature and humidity sensing [10], [11], vital sign monitoring [12], [13] and critical asset inspection [14], [15].

The tag in a typical HR setting has no power source of its own (i.e., it is passive) and, in its simplest form, it is just an antenna in series with a diode [16], [17]. In the uplink, a node containing a radio transmitter (the Tx) sends a bandpass signal that illuminates the tag, inducing a voltage across the diode that in turn produces a multiband current according to the nonlinear diode equation. This results in a weak re-radiated signal at harmonics of the the incident wave frequency (now the fundamental frequency). A node containing a receiver (the Rx) detects this downlink return signal, typically processing only the second harmonic, which is usually the strongest. Because the return signal is so weak, the operational range is limited, which often becomes the central problem in the system design. In more detail, the second-harmonic downlink signal emitted by the tag has power proportional to the square of the power of the incident uplink signal, except at extremely close range. When combined with the typical inverse-square law dependence on distances in the uplink and downlink, it gives the overall signal power response from Tx to a co-located Rx an inverse sixth-power law [1]. The result is a very short range. For instance, in [18] a system using classical dipole-based tags was shown to have a detection range of up to 40 m when operating in the S-band (2.9/5.8 GHz) with 13dBi Tx/Rx antennas and an output power of 3 W, and up to 15 m at 10 W with 15dBi antennas in the X-band (9.3/18.6 GHz). In contrast, harmonic RFID systems often employ extra circuitry at the tag to allow for additional modulation and, possibly, amplification of the backscattered signal [8], [9]. This, however, increases the requirements to the incident power level at the tag which limits the range even further prompting the move to the lower operational frequencies in the UHF range.

Generally, the usual approach to increase the range is to increase the Tx power. Unfortunately, the resulting range improvement in HR is modest: when the tag's approximate power-squaring action is combined with the inverse fourth-power distance dependence, the range varies as the cube root of any Tx power increase. For example, an 8-fold increase in Tx power results in a corresponding range increase factor of just $\sqrt[3]{8} = 2$. Nevertheless, it is common to employ a very powerful transmitter or a high gain antenna at the Tx, or both the Tx and

Manuscript received April 22, 2021; revised September 29, 2021 and March 23, 2022; accepted March 29, 2022. Date of publication April 1, 2022; date of current version April 26, 2022. The associate editor coordinating the review of this manuscript and approving it for publication was Dr. Bo Tang. This work was supported in part by the Royal Society of New Zealand via Catalyst: Seeding under Grant CSG-FRI1802, and in part by the Scion Postdoctoral Scholarship under Grant S07084. *(Corresponding author: Anastasia Lavrenko.)*

Anastasia Lavrenko was with Scion (New Zealand Forest Research Institute), Christchurch 8041, New Zealand. He is now with the University of Twente, 7500 AE Enschede, Netherlands (e-mail: a.lavrenko@utwente.nl).

James K. Cavers is with the Wireless Research Centre, University of Canterbury, Christchurch 8140, New Zealand, and also with the School of Engineering Science, Simon Fraser University, Burnaby BC K1S 5B6, Canada (e-mail: cavers@sfu.ca).

Graeme K. Woodward is with the Wireless Research Centre, University of Canterbury, Christchurch 8140, New Zealand (e-mail: graeme.woodward@canterbury.ac.nz).

Digital Object Identifier 10.1109/TSP.2022.3164183

Rx, as a brute force way to increase the range. Examples of such high-power solutions include 25 kW systems in [19], [20]; 4 kW and 3 kW systems in [21] and [22], respectively; and, most recently, a 1 kW system in [23].

We take an alternative, and novel, approach to increasing the range of harmonic radar. Recently, we proposed the use of auxiliary Tx nodes, which we term "helper nodes" [24]. Although they transmit only simple tones, they provide a significant increase in average power of the desired signal at Rx, and therefore allow a greater range or lower antenna gain, while being far simpler and less costly than the high-power Tx. Helpers can also be added incrementally to achieve desired range and/or SNR increase. Consider for a instance a single ranging node (RN) designed for a given range supported by one, or several, helpers. As the range requirements increase, more helpers can be deployed without changing the RN. Further, in a helper-assisted system the total transmit power is distributed among helpers and RN, so that phase noise skirts and parasitic harmonic leakage do not impair an RN's operation in the downlink.

The operation of a helper-based system is enabled by the nonlinear action of the tag that produces intermodulation terms when excited by multiple signal sources. Since the power of the intermodulation terms is defined by the product of the ranging signal and the helper node contribution, using it for ranging offers an opportunity for boosting the tag output. In a basic configuration, the helper tones are allowed to arrive at the tag noncoherently. Most of the time, this provides a significant increase in average power of the desired signal at the Rx. During occasional phase misalignments, however, the received power can be very low. In this paper, we show how the helper tones can instead be made to arrive coherently at the tag, thereby maximizing the power of the tag downlink and, in turn, maximizing the Rx signal power and/or the range. In the following, we describe the adaptive phase coherence algorithm in detail, and provide an analysis of the resulting Markovian growth of signal power. We analyze the performance improvement on an example of a practically built conventional system and explain the implications for the system designs.

The general concept of a multi-tone harmonic radar that uses the intermodulation product at the output of a non-linear target has been previously explored in [25]–[27]. However, to the best of our knowledge there has been no prior work on the use of the intermodulation products of multiple helper transmitters to increase the downlink power from a passive, non-linear tag. Somewhat related is a design for backscatter data communication [28], in which a desired data signal from a Tx arrives at a separate Rx, as does a simple tone from a third node (the exciter), resulting in beneficial interference at the Rx that puts the composite signal in a higher-gain region of the noncoherent detector. In contrast, our helper-node method performs ranging in harmonic radar at twice the carrier frequency of the uplink, the tag is simple and entirely passive, and the intermodulation component produced by helper tones is the essential part of the received signal.

In what follows, Section II outlines the physical and signalling layout of the HR system. Section III then contrasts performance with phase-coherent helper nodes against brute force increase of Tx power. Section IV defines the phase-coherence algorithm, and Section V provides the analyses of convergence, performance effects of the result, and limitations of the helper-node method. Section VI then demonstrates the degree of improvement due to helper nodes for a specific implementation of a Tx-Rx ranging node. Finally, Section VII presents our conclusions about the helper-node method and what the next steps might be.

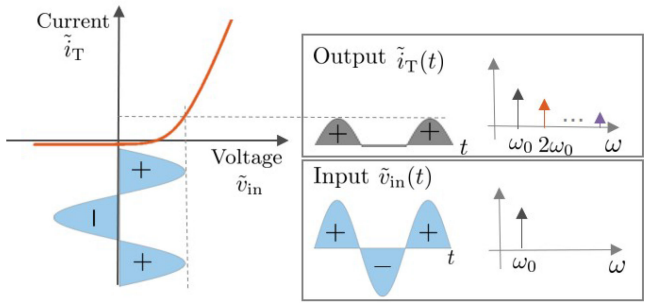

Fig. 1. Relationship between the input voltage and the output current of a harmonic radar tag, in time and frequency.

II. Harmonic Radar

A. Conventional Harmonic Radar

In classical radar, the radar transmitter emits a radio frequency (RF) pulse at frequency $\omega_0 = 2\pi f_0$ and the radar receiver listens for reflections from a passive target at the same frequency. In contrast, a HR target is nonlinear, as well as passive, so its response is rich in harmonics. Typically, such a harmonic response is induced by attaching a battery-less harmonic transponder tag to the target of interest. HR tags typically combine a resonant antenna, a low-voltage diode and possibly a simple impedance matching network [16], [17], [21]. The antenna voltage drives the diode, creating a rectified current that contains harmonics of the received signal, as sketched in Fig. 1. The second harmonic is usually the strongest, so the tag's transmit antenna is tuned to $2\omega_0$. The second harmonic signal is thus emitted from the tag and subsequently detected at the HR receiver. The main advantage of harmonic operation is that the background clutter is greatly reduced, since RF reflection from most objects is linear, producing a backscattered response only at ω_0.

Below, we provide a model of conventional HR that combines the effects of the uplink (HR transmitter to tag antenna input), the tag (tag antenna input, nonlinearity and tag antenna output), and the downlink (tag antenna output to the HR receiver). We assume for simplicity that the HR transmitter is collocated with the HR receiver, forming a single HR node (the ranging node, or RN). Note that ranging systems can have more than one RN, e.g., in order to locate the tag by multilateration. For simplicity of presentation, our analysis considers just one. Throughout, we distinguish real bandpass signals from their complex envelopes by an overhead tilde; for example, we denote the real bandpass signal transmitted at ω_0 by $\tilde{s}(t) = \mathrm{Re}\{s(t)e^{\jmath\omega_0 t}\}$ and its baseband complex envelope by $s(t)$.

In the uplink, the RN sends a pulse with complex envelope

$$s_{\rm r}(t) = \sqrt{2P_{\rm r}R_{\rm tx}}x(t), \tag{1}$$

where $P_{\rm r}$ is the transmit RF power and $R_{\rm tx}$ is the transmit antenna resistance. We assume that $x(t)$ occupies the RN's pulse duration $[0, T_{\rm r}]$, where it satisfies $|x(t)| = 1$, and has good autocorrelation properties. Examples include biphase ± 1 sequences or chirps (linearly frequency modulated pulses). With line of sight transmission, the RN signal is received at the tag antenna with the complex envelope

$$v_{\rm in}(t) = \sqrt{k_{\rm in}\frac{|Z_{\rm F}|}{R_{\rm tx}}G_{\rm tx}}h_{\rm u}(d_{\rm r})s_{\rm r}(t-\tau_{\rm r})e^{\jmath\theta_{\rm r}}, \tag{2}$$

in which $Z_{\rm F}$ and $k_{\rm in}$ are the tag antenna impedance and the input tag power transfer efficiency at ω_0, respectively, $G_{\rm tx}$ is the transmit antenna gain, and $h_{\rm u}(d_{\rm r}) = \sqrt{G_{\rm tag}(\omega_0)c^2/(2\omega_0 d_{\rm r})^2}$ is the uplink gain where $G_{\rm tag}(\omega)$ denotes the tag antenna gain, c is the speed of light, and $d_{\rm r}$ the distance from the RN to the tag. The phase of $Z_{\rm F}$ has been omitted since fixed phase shifts do not affect the phase adaptation algorithm presented in Sections IV and V. The propagation delay is $\tau_{\rm r} = d_{\rm r}/c$ and the corresponding phase shift is $\theta_{\rm r} = -\omega_0\tau_{\rm r}$. For notational convenience, we combine (1) and (2) to obtain an alternative expression for the input voltage at the tag as

$$v_{\rm in}(t) = A_{\rm r}x(t-\tau_{\rm r})e^{\jmath\theta_{\rm r}}, \tag{3}$$

where $A_{\rm r} = \sqrt{2|Z_{\rm F}|k_{\rm in}P_{\rm r}G_{\rm tx}}h_{\rm u}(d_{\rm r})$.

The tag can be modeled as a series circuit with the real bandpass voltage $\tilde{v}_{\rm in}(t) = {\rm Re}\{v_{\rm in}(t)e^{\jmath\omega_0 t}\}$ as input and real multiband current $\tilde{i}_{\rm T}(t)$ as response, linked by the nonlinear equation

$$\frac{\tilde{v}_{\rm in}(t)}{n_{\rm i}V_{\rm T}} = \rho\frac{\tilde{i}_{\rm T}(t)}{I_{\rm s}} + \ln\left(\frac{\tilde{i}_{\rm T}(t)}{I_{\rm s}} + 1\right). \tag{4}$$

Here, $n_{\rm i}$ and $V_{\rm T}$ are diode thermal voltage and the ideality factor, respectively, $I_{\rm s}$ is its saturation current and $\rho = I_{\rm s}|Z_{\rm F}|/n_{\rm i}V_{\rm T}$. An explicit solution to (4) has been obtained in [29] in terms of the Lambert W-function. From that, [29] also provides the closed-form expressions for the relation between the complex envelope $v_{\rm in}(t)$ at the fundamental frequency ω_0 and the complex envelope $i_2(t)$ of the current at the second harmonic $2\omega_0$, in two conditions:

- small-signal conditions $(v_{\rm in}(t)/n_i V_{\rm T} < -1 - \ln\rho - \rho)$, where

$$i_2(t) \approx \frac{b_{\rm t}}{|Z_{\rm F}|}v_{\rm in}^2(t), \tag{5}$$

  in which $b_{\rm t} = \frac{1}{4(n_i V_{\rm T})}\sum_{n=1}^{\infty}((-1)^{n-1}n^{n+1}/n!)\rho^n e^{n\rho}$. For $\rho < 0.04$ it simplifies further to $b_{\rm t} \approx \rho/4n_{\rm i}V_{\rm T}$;
- large-signal conditions $(v_{\rm in}(t)/n_i V_{\rm T} \gg 1)$, where

$$i_2(t) \approx \frac{2}{3\pi}\frac{1}{|Z_{\rm F}|}|v_{\rm in}(t)|e^{\jmath 2\varphi_{\rm in}(t)}, \tag{6}$$

  in which $\varphi_{\rm in}(t) = \arg(v_{\rm in}(t))$.

From (5) and (6), the phase of the tag output current at the second harmonic is double that of the input signal, while its magnitude grows quadratically in the small-signal region and linearly in large signal conditions. Our principal interest is to extend the limits of the operating range where signals at the tag are weak. Consequently, in the following we consider the small-signal quadratic[1] model (5).

With $Z_{\rm H}$ as the output impedance of the tag at $2\omega_0$, the complex envelope of the tag output voltage in the small-signal conditions becomes

$$v_{\rm out} = |Z_{\rm H}|i_2(t) \approx \frac{|Z_{\rm H}|}{|Z_{\rm F}|}b_{\rm t}v_{\rm in}^2(t), \tag{7}$$

with the corresponding bandpass equivalent provided by $\tilde{v}_{\rm out}(t) = (b_{\rm t}|Z_{\rm H}|/|Z_{\rm F}|){\rm Re}\{v_{\rm in}^2(t)e^{\jmath 2\omega_0 t}\}$. Note that for the rest of the paper, we drop the approximation sign in (7), bearing in mind that it is a small-signal approximation.

Finally, the downlink mirrors the uplink, such that at the HR receiver we obtain

$$r(t) = h_{\rm d}(d_{\rm r})\sqrt{k_{\rm out}\frac{R_{\rm rx}}{|Z_{\rm H}|}G_{\rm rx}}v_{\rm out}(t-\tau_{\rm r})e^{\jmath 2\theta_{\rm r}} + n(t), \tag{8}$$

where $G_{\rm rx}$ is the receiver antenna gain and $h_{\rm d}(d_{\rm r}) = \sqrt{G_{\rm tag}(2\omega_0)c^2/(4\omega_0 d_{\rm r})^2}$ is the downlink gain, in which $R_{\rm rx}$ is the resistance of the Rx antenna and $k_{\rm out}$ is the output tag power transfer efficiency at $2\omega_0$. The complex noise $n(t)$ in (8) is considered to be white Gaussian with power spectral density (PSD) $N_0 = R_{\rm rx}k_{\rm B}T_{\rm n}$ where $k_{\rm B}$ is the Boltzman constant and $T_{\rm n}$ is the noise temperature. Lastly, we combine (7), (8) and (3) to obtain

$$r(t) = \eta_{\rm r}A_{\rm r}^2x^2(t-2\tau_{\rm r})e^{\jmath 4\theta_{\rm r}} + n(t), \tag{9}$$

where $\eta_{\rm r} = h_{\rm d}(d_{\rm r})b_{\rm t}\sqrt{|Z_{\rm H}|R_{\rm rx}k_{\rm out}G_{\rm rx}}/|Z_{\rm F}|$. The product $\eta_{\rm r}A_{\rm r}^2$ represents the total gain of the Tx–tag–Rx link. In the absence of noise, (2), (7) and (8) combined make the received amplitude $|r(t)|$ proportional to $h_{\rm u}^2(d_{\rm r})h_{\rm d}(d_{\rm r})$, and hence inversely proportional to $d_{\rm r}^3$. The received power in harmonic radar with battery-less passive tags descried by (4) is then inversely proportional to $d_{\rm r}^6$, i.e., an inverse sixth-power law.

B. Distributed HR System With Auxiliary (Helper) Nodes

Consider the system of [24] that, in addition to the RN of a conventional HR system, employs M auxiliary transmitters, each sending a simple tone at ω_0 (see Fig. 2). For simplicity, we assume that these additional nodes, which we also refer to as helper nodes (HNs) or simply helpers, have the same transmit power and antenna gains which we denote by $P_{\rm h}$, $G_{\rm h}$, respectively. Then, when the m-th helper sends the complex envelope $s_m = \sqrt{2P_{\rm h}R_{\rm tx}}e^{\jmath\theta_m}$, where θ_m denotes its local oscillator (LO) phase relative to that of the RN, the tag receives

$$v_{\rm in}(t) = \sqrt{k_{\rm in}\frac{|Z_{\rm F}|}{R_{\rm tx}}G_{\rm tx}}h_{\rm u}(d_{\rm r})s_{\rm r}(t-\tau_{\rm r})e^{\jmath\theta_{\rm r}} + \sqrt{2k_{\rm in}P_{\rm h}G_{\rm h}|Z_{\rm F}|}\sum_{m=1}^{M}h_{\rm u}(d_m)e^{\jmath\bar{\theta}_m}. \tag{10}$$

[1]Our numerical results in Section VI-C show that the phase-adaptation approach that we develop based on the small-signal model continues to work well in the tag regions above quadratic.

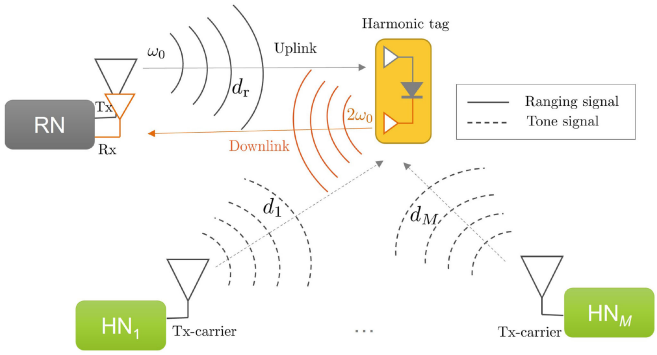

Fig. 2. Harmonic radar system with auxiliary helper nodes: a single ranging node (RN) that transmits a ranging signal at ω_0 and listens for signal returns at $2\omega_0$ is aided by M helper nodes (HNs) that transmit simple tones at ω_0.

Here, d_m denotes the distance between the m-th helper node and the tag, while $\bar{\theta}_m = \theta_m - \omega_0\tau_m = \theta_m - \omega_0 d_m/c$. With the notation of (3), (10) becomes

$$\begin{aligned} v_{\rm in}(t) &= A_{\rm r}x(t-\tau_{\rm r})e^{\jmath\theta_{\rm r}} + \sum_{m=1}^{M} A_{{\rm h},m}e^{\jmath\bar{\theta}_m} \\ &= A_{\rm r}x(t-\tau_{\rm r})e^{\jmath\theta_{\rm r}} + A_{\rm h}e^{\jmath\theta_{\rm h}}, \end{aligned} \tag{11}$$

where $A_{{\rm h},m} = \sqrt{2|Z_{\rm F}|k_{\rm in}P_{\rm h}G_{\rm h}}h_{\rm u}(d_m)$. We distinguish here the RN contribution, $A_{\rm r}x(t-\tau_{\rm r})e^{\jmath\theta_{\rm r}}$, and the HN contribution, $A_{\rm h}e^{\jmath\theta_{\rm h}} = \sum_{m=1}^{M} A_{{\rm h},m}e^{\jmath\bar{\theta}_m}$. Substituting (11) into (7) gives the tag output as

$$\begin{aligned} v_{\rm out}(t) &= \frac{|Z_{\rm H}|}{|Z_{\rm F}|}b_{\rm t}v_{\rm in}^2(t) \\ &= \frac{|Z_{\rm H}|}{|Z_{\rm F}|}b_{\rm t}\left(A_{\rm r}x(t-\tau_{\rm r})e^{\jmath\theta_{\rm r}} + A_{\rm h}e^{\jmath\theta_{\rm h}}\right)^2, \end{aligned} \tag{12}$$

and inserting (12) into (8) finally yields

$$\begin{aligned} r(t) = \eta_{\rm r}\Big(&A_{\rm r}^2x^2(t-2\tau_{\rm r})e^{\jmath 2\theta_{\rm r}} + 2A_{\rm r}A_{\rm h}x(t-2\tau_{\rm r})e^{\jmath(\theta_{\rm r}+\theta_{\rm h})} \\ &+A_{\rm h}^2e^{\jmath 2\theta_{\rm h}}\Big)e^{\jmath 2\theta_{\rm r}} + n(t). \end{aligned} \tag{13}$$

The composition of the downlink signal (13) captures the nonlinear action of the tag in its quadratic regime near the maximum range. The received signal now contains three terms:

1) the first term (ranging signal only) corresponds to the output of a conventional HR system without helpers;
2) the second term (intermodulation) carries the ranging waveform $x(t)$ with amplitude proportional to $2A_{\rm r}A_{\rm h}$;
3) the third term (helpers only) is unmodulated carrier.

In helper-based HR, the receiver detects the intermodulation term (term 2 above) because its power is at least 6 dB greater than in conventional HR (term 1), if the sum of the helper tones exceeds the RN amplitude ($A_{\rm h} \geq A_{\rm r}$). Our design goal is then to maximize the probability that amplitude $A_{\rm h}$ of the helper node sum exceeds that of RN, and, conversely, to minimize the possibility that it falls below it. Detection of term 2 alone is possible because the receiver's sliding correlator or filter matched to $x(t)$ is unresponsive to the other two terms, since the first term contains $x^2(t) = 1$ and the third term is a constant, neither of which correlate strongly against typical $x(t)$ sequences with good autocorrelation properties. Thus, with term 2 as the objective in (13), the main goal of the helper-based HR system design is maximizing the amplitude of the helper node contribution $A_{\rm h}$.

Discussion above focused on transmit powers $P_{\rm r}$ and $P_{\rm h}$. However, $A_{\rm r}$ in (3) and $A_{\rm h}$ in (11) show that, in both RN and helpers, it is their respective effective isotropic radiated powers (EIRPs), $P_{{\rm e,r}} = P_{\rm r}G_{\rm tx}$ and $P_{{\rm e,h}} = P_{\rm h}G_{\rm h}$, that affect strength of signals arriving at the tag. This allows a familiar design trade-off between transmit power and antenna gain, although increasing either of them usually incurs greater size, weight and cost.

III. Benefits of Using Helper Nodes

Above, we saw that when the amplitude $A_{\rm h}$ of the HN contribution is greater than half of the ranging signal amplitude $A_{\rm r}$, helper-based system provides an increased SNR (or range), relative to conventional HR. The advantage of employing helper nodes is that the increase of the tag output power is achieved by using simple constant-envelope signals, which are inexpensive and power-efficient. Further, helper nodes can be added incrementally in order to provide the power boost needed for the desired SNR or range increase. It is worth noting that in some systems, helpers may be distributed around the operating area independently of the locations of the RN and the tag. Some of them may then be closer to the tag than is the RN, thereby producing a much larger downlink signal than would be achievable by increasing Tx power of the RN instead. Below, we evaluate how much improvement can be achieved with helper nodes in different operating schemes.

A. Coherent Transmission Scheme

A coherent transmission scheme ensures that HN signals arrive at the tag in phase, in spite of drifts in distances and in oscillator phases. In Section IV, we introduce an adaptive phase coherence method to achieve such a system. Here, we show that the benefits of coherent operation are substantial. Consider the amplitude $A_{\rm h}$ of the helper node contribution introduced in (11):

$$A_{\rm h} \triangleq \left|\sum_{m=1}^{M} A_{{\rm h},m}e^{\jmath\bar{\theta}_m}\right|. \tag{14}$$

If all $\bar{\theta}_m = \bar{\theta}$, then

$$A_{\rm h} = \left|e^{\jmath\bar{\theta}}\sum_{m=1}^{M} A_{{\rm h},m}\right| = \sum_{m=1}^{M} A_{{\rm h},m} = MA, \tag{15}$$

where the last equality assumes, for simplicity of presentation in this section, that all helper tones arrive at the tag with the same amplitude A. Then, the power of the intermodulation term in (13) is proportional[2] to

$$P_{\rm i} = 4\,M^2A^2A_{\rm r}^2, \tag{16}$$

[2]For notational convenience, here and in the following the signal power is assumed to be normalised to the total link gain $\eta_{\rm r}$ defined below (9).

which is $4\,M^2\alpha^2$ times the power of the ranging signal in a conventional HR system (first term in (13)) where $\alpha = A/A_{\rm r}$ is the ratio of the HN and RN amplitudes at the tag. As a result, the helper-based system provides an SNR boost of $20\log(M\alpha) + 6$ dB. Since received signal power in HR varies as inverse sixth power of distance, a coherent helper system provides a range extension factor (REF) of

$$\zeta_{\rm coh} = (4\,M^2\alpha^2)^{1/6} = \sqrt[3]{2\,M\alpha}. \tag{17}$$

The value of the amplitude ratio α will depend on the ratio of the EIRP of the ranging transmitter, $P_{\rm e,r} = P_{\rm r}G_{\rm tx}$, and HNs, $P_{\rm e,h} = P_{\rm h}G_{\rm h}$, in the direction of the tag, as well as the distances $d_{\rm r}$, $d_{\rm m}$ via the uplink and downlink gains. Assuming all path losses to be equal, the amplitude ratio becomes $\alpha = \sqrt{P_{\rm e,h}/P_{\rm e,r}}$ which turns into $\alpha = \sqrt{G_{\rm h}/G_{\rm tx}}$ if we further assume equal transmit powers at the RN and HNs. In a typical setting, the helper nodes would carry broadbeam[3] antennas to avoid the need for manual or electronic scanning. As for the RN antenna gain $G_{\rm tx}$, it is often assumed to be relatively large to enable tag localization (hence $\alpha \ll 1$ or $\alpha \approx 1$ if helper antenna gains are also high). On the other hand, in a system that solely relies on ranging and multilateration for tag localization, such as in [30] for instance, the RN antennas can be more broadbeam ($\alpha \approx 1$). A combination of multiple RNs with pointing and multilateration is also possible.

Expression (17) implies that with equal path losses and EIRPs ($\alpha = 1$) $M = 4$ helper nodes can double the range, compared to conventional HR. Furthermore, with all things being equal, even for the simplest case, i.e., a single helper ($M = 1$) where coherence is no longer a consideration, REF is 1.26 which means a 26% increase in range for almost no effort. This range increase can be decisive. Consider for example tracking of insects or small vertebrates. Movement of the RN or helpers might startle the subject and change its behavior. Extending the system's range, e.g., from 20 m to 25 m, can mitigate the problem. Another example is discovering and locating victims trapped in rubble after an avalanche or an earthquake. Being able to increase the effective power impinging on the locator circuitry, and therefore the search range, can make a crucial difference to the victim's chances of survival.

B. Basic Scheme – Noncoherent Transmission

Although the focus of this paper is ensuring that helper tones arrive coherently at the tag, there may be a role for a simpler noncoherent system, one which omits the adaptive phase coherence algorithm, as in [24]. According to (14), if the phases $\bar{\theta}_m$ are mutually independent and uniformly distributed in $[-\pi, \pi)$, then the mean helper node power at the tag is the power-wise sum

$$\bar{P}_{\rm h} = \sum_{m=1}^{M} A_{{\rm h},m}^2 = MA^2, \tag{18}$$

where the last equality, for simplicity, sets all helper amplitudes equal to A. The mean power of the intermodulation term then becomes

$$\bar{P}_{\rm i} = 4\bar{P}_{\rm h}A_{\rm r}^2 = 4\,MA_{\rm r}^4\alpha^2. \tag{19}$$

This is $4M\alpha^2$ times the power of the signal term in a conventional HR system. On the other hand, this average is M times smaller than the constant power (16) of the coherent transmission. At the mean power of the intermodulation term (19), the SNR boost is then $10\log(M\alpha) + 6$ dB.

What about the instantaneous power $P_{\rm i} = 4A_{\rm h}^2A_{\rm r}^2$? From (14), the magnitude $A_{\rm h}$ varies as the individual phases drift with changing distances to the tag and different individual LO phase offsets. Suppose that there are many helpers. Then, invoking the central limit theorem we can model the real and imaginary components of the helper node contribution as Gaussian variables with weak mutual dependence. It is well known that the resulting complex Gaussian process has a Rayleigh distributed amplitude ($A_{\rm h}$) and an exponentially distributed power ($P_{\rm h} = A_{\rm h}^2$) [31]. Consequently, the cumulative distribution function (CDF) of $P_{\rm i}$ for many helpers is asymptotically

$$\Pr[P_{\rm i} \le z] = 1 - e^{-\frac{z}{\bar{P}_{\rm i}}} = 1 - e^{-\frac{z}{4\,MA_{\rm r}^4\alpha^2}}. \tag{20}$$

From (20), the instantaneous power of the helper-based HR system with noncoherent transmissions is $4M\alpha^2$ times the power of conventional HR approximately 37% of the time, and when the phases are almost aligned it can occasionally approach the power of coherent transmission, which is $4\,M^2\alpha^2$ times that of conventional HR. However, infrequent deep fades can take it *below* the power of conventional HR, with probability $1 - \exp(-1/4M\alpha^2) \approx 1/4M\alpha^2$. In other words, this means that if the range is extended by a factor $\zeta_{\rm inc}$, then the dropout probability becomes $1 - \exp(-\zeta_{\rm inc}^6/4M\alpha^2)$ which grows rapidly. For such a system, range extension may not be an appropriate measure. Instead, if this noncoherent system operates at the same range as conventional HR, it provides much higher SNR on average, at the cost of dropouts a $1/(4M\alpha^2)$ fraction of the time.

C. Brute Force Conventional HR

A helper-based system invests the power of the ranging node and M helpers into SNR improvement or range increase. Assume, again for simplicity, that all helpers have the same transmit power as the ranging node and that all path losses are equal. A fair comparison might then allow conventional HR to increase its transmit power by a factor of $M + 1$. With this brute-force improvement, the received power at the tag in conventional HR is

$$P_{\rm r} = (M+1)^2A_{\rm r}^4. \tag{21}$$

Comparison with (16) and consideration of the inverse sixth power dependence on range gives the REF as

$$\zeta_{\rm conv} = \sqrt[3]{M+1}. \tag{22}$$

[3]Note that broadbeam, and even omnidirectional, antennas may obtain high gain by compressing the beam in the vertical (elevation) direction.

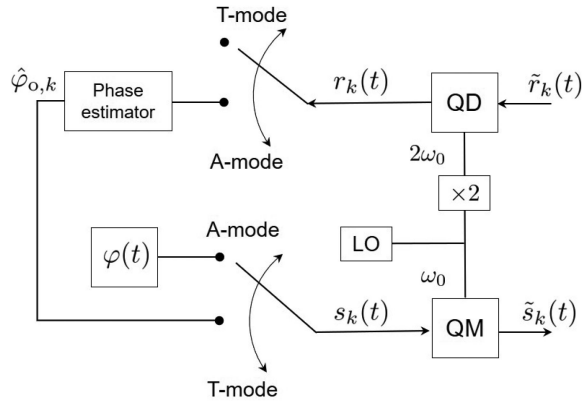

Fig. 3. Block scheme of a helper node that can operate in one of two modes: a phase adjustment mode (A) or a fixed-phase transmission mode (T). QM and QD here stand for the quadrature modulator and demodulator, respectively.

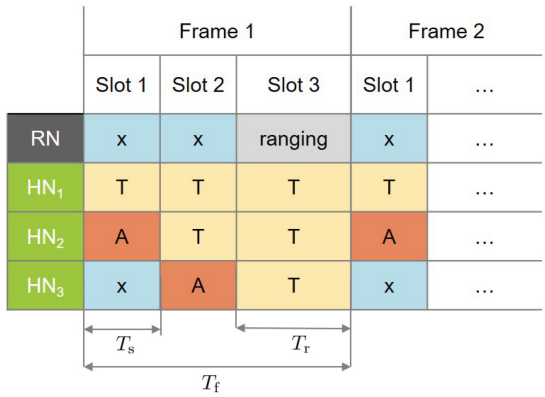

Fig. 4. Simplified transmission frame structure for $M = 3$ helper nodes. The frame T_f is organized in M time slots: $M - 1$ phase adjustment slots of duration T_s each followed by a T_r-long slot for ranging, i.e., $T_f = (M - 1)T_s + T_r$. .

For a single helper ($M = 1$), therefore, SNR and REF of the conventional HR system are as good as those of the coherent helper-based system (16) in which $\alpha = 1$. However, conventional HR rapidly falls behind the coherent helper system as the number of helper nodes increases, leaving the coherent system with an asymptotic $(26 \cdot \alpha)\%$ greater range. On the other hand, to match the range of a helper-based system, the conventional system must increase the transmit power of its RN, which also increases the weight and cost of the amplifier and power supply. It is worth noting here that HR systems have increased linearity requirements on the RN in order to minimize the parasitic 2nd harmonic leakage, leading to the need for more carefully designed amplifiers and, depending on the modulation, implementation of additional linearization techniques [32], [33]. In contrast, the helper-node approach is distributed and incremental, so that helpers can be added as needed. Also, the set of helper nodes boosts the effective power of every RN, in case there is more than one.

IV. Phase Adaptation for Coherent Helper Node Signal Combining At the Tag

A. Two-Mode Transmission With Phase Adjustment

From Section II-B, helper nodes transmit a fixed-phase tone, a mode which we will call T-mode (tone). However, from (16) and (17), we want the individual helper node tones to combine coherently at the tag, in order to maximize the tag's output power. That requires an additional mode (A, for adjustment) in which a helper node adjusts its transmit phase θ_m in response to the tag output signal $\tilde{v}_{\text{out}}(t)$, which implies that helper nodes must also be able to receive signals on the downlink. Fig. 3 outlines the helper node structure that supports this two-mode operation. When in mode A, the helper node sweeps its phase around the circle as $\theta_m + \varphi(t)$, where $\varphi(t) = 2\pi t/T_s, 0 \le t \le T_s$ and T_s is the phase sweep duration. During this time, it processes the received response from the tag in order to calculate the new value of transmit phase to use when it next returns to T mode.

To coordinate the change between the two different modes at each helper and the operation of the ranging node, the transmission time consists of a series of frames, e.g., see Fig 4. Maintaining such a frame structure and its use requires a higher protocol layer on a different frequency, or perhaps on a wired network if there is one among all nodes. The protocol would provide three principal services:

- Establish slotting (determination of the time intervals). The timing can be possibly derived from a satellite reference via GPS or a master clock that could be associated with the RN.
- Coordinate use of slots by all nodes, including plug and play operation in which helper nodes and RNs can be introduced to or removed from the network. Assigning nodes to slots may include sorting by amplitude (see Section V-B).
- If there are multiple RNs, allow them to report their ranging information to some central point for processing.

We note that even for a conventional (non-helper) HR system with more than one RN, a protocol for coordinating the RNs and reporting of measurements would be similar [30].

Every frame begins with a phase adjustment interval of $M - 1$ time slots, each of duration T_s, used for helper phase adjustments, followed by a ranging interval of duration T_r, resulting in a total frame duration of $T_f = (M - 1)T_s + T_r$. Furthermore, during phase adjustment slots only a single helper is in mode A at any given time. Fig. 4 exemplifies a simple frame structure for $M = 3$ helpers. In slot 1, helper 1, which is in mode T, sends a tone and helper 2, in mode A, sends a phase sweep that allows it to align its phase with that of helper 1. In slot 2, helpers 1 and 2 send their now-aligned tones in mode T, while helper 3, in mode A, sends the phase sweep in order to align its phase with that of the sum of helpers 1 and 2. The adjustment interval continues to add one helper at a time, slot by slot, until all M helpers are aligned. In the absence of receiver noise, $M - 1$ phase adjustment slots are sufficient here to achieve exact phase coherence. During the ranging interval that follows (slot 3 in Fig. 4), the RN sends the ranging signal while the helpers, all now in mode T, send tones which arrive coherently at the tag, thereby boosting the amplitude of the intermodulation term at the tag output.

In more detail, helper m adjusts its phase in slot $i = m-1, m \in [2, M]$, which lasts over $(m-2)T_\mathrm{s} \le t \le (m-1)T_\mathrm{s}$. The signal arriving at the tag consists of the phase-sweep of helper m and the fixed-phase tones of helpers 1 to $m-1$. The complex envelope of the tag input is then

$$v_\mathrm{in}(t-(m-2)T_\mathrm{s}) = A_{\mathrm{h},m} e^{\jmath\bar{\theta}_m} e^{\jmath\varphi(t-(m-2)T_\mathrm{s})} + A_{\mathrm{p},m-1} e^{\jmath\theta_{\mathrm{p},m-1}}, \tag{23}$$

where $A_{\mathrm{p},m-1} e^{\jmath\theta_{\mathrm{p},m-1}} = \sum_{m=1}^{m-1} A_{\mathrm{h},m} e^{\jmath\bar{\theta}_m}$ is the partial sum of helper node signals in slot $i = m-1$, inherited from the adjustment in the previous slot. Note that only a subset of helpers is in T mode during any phase adjustment slot. After the final adjustment by helper M in slot $i = M-1$, the sum is no longer partial so that $A_\mathrm{h} e^{\jmath\theta_\mathrm{h}} = A_{\mathrm{p},M} e^{\jmath\theta_{\mathrm{p},M}}$. Moving to the downlink, (12) gives the second-harmonic complex envelope at the tag output in slot $i = m-1$ for helper m as

$$v_\mathrm{out}(t-(m-2)T_\mathrm{s}) = (|Z_\mathrm{H}|/|Z_\mathrm{F}|) b_\mathrm{t} v_\mathrm{in}^2(t-(m-2)T_\mathrm{s}). \tag{24}$$

Substituting now (23) into (24), the second-harmonic receiver input at helper m, which is in mode A, is given by

$$\begin{aligned} r_m(t-(m-2)T_\mathrm{s}) = \eta_m \Big(& A_{\mathrm{h},i+1}^2 e^{\jmath 2\bar{\theta}_m} e^{\jmath 2\varphi(t-(m-2)T_\mathrm{s})} \\ & + 2A_{\mathrm{h},m} A_{\mathrm{p},m-1} e^{\jmath(\bar{\theta}_m + \theta_{\mathrm{p},m-1})} e^{\jmath\varphi(t-(m-2)T_\mathrm{s})} \\ & + A_{\mathrm{p},m-1}^2 e^{\jmath 2\theta_{\mathrm{p},m}} \Big) e^{-\jmath 2\omega_0 \tau_{m-1}} + n_m(t-(m-2)T_\mathrm{s}), \end{aligned} \tag{25}$$

where $\eta_m = h_\mathrm{d}(d_m) b_\mathrm{t} \sqrt{k_\mathrm{out} |Z_\mathrm{H}| R_\mathrm{rx}} / |Z_\mathrm{F}|$. For simplicity, in (23)–(25) we ignore the propagation delay in $\varphi(t)$, on the grounds that $\tau_m \ll T_\mathrm{s}$, but we revisit this point later in Section V-D. From (24), the partial sum $A_{\mathrm{p},m-1}$ from slot $m-1$ reflects adjustments by the $m-1$ prior helpers, so that helper m should change its phase to equal that of the partial sum, $\theta_{\mathrm{p},m-1}$. In the absence of error, this maximizes the amplitude of the next partial sum $A_{\mathrm{p},m} = A_{\mathrm{h},m} + A_{\mathrm{p},m-1}$. According to (25), helper m can achieve this by offsetting its phase by

$$\varphi_{\mathrm{o},m} = \theta_{\mathrm{p},m-1} - \bar{\theta}_m = \theta_{\mathrm{p},m-1} - \theta_m + \omega_0 \tau_m. \tag{26}$$

Below, we describe how $\varphi_{\mathrm{o},m}$ can be estimated from the received signal $r_m(t-(m-2)T_\mathrm{s})$.

B. Phase Offset Estimation

The individual terms in (25) are separable with respect to $\varphi(t)$ via the following integrals:

$$\begin{aligned} G_{0,m} &= \int_{(m-2)T_\mathrm{s}}^{(m-1)T_\mathrm{s}} r_m(t)\mathrm{d}t \\ &= \underbrace{\eta_m T_\mathrm{s} A_{\mathrm{p},m-1}^2 e^{\jmath 2(\theta_{\mathrm{p},m-1} - \omega_0\tau_m)}}_{\dot{G}_{0,m}} + \int_{(m-2)T_\mathrm{s}}^{(m-1)T_\mathrm{s}} n(t)\mathrm{d}t \\ &= \dot{G}_{0,m} + n_{0,m}, \end{aligned} \tag{27}$$

$$G_{1,m} = \int_{(m-2)T_\mathrm{s}}^{(m-1)T_\mathrm{s}} r_m(t) e^{-\jmath 2\pi \frac{t-(m-2)T_\mathrm{s}}{T_\mathrm{s}}} \mathrm{d}t \tag{28}$$

$$\begin{aligned} &= \underbrace{2\eta_m T_\mathrm{s} A_{\mathrm{h},m} A_{\mathrm{p},m-1} e^{\jmath(\bar{\theta}_m + \theta_{\mathrm{p},m-1} - 2\omega_0\tau_m)}}_{\dot{G}_{1,m}} \\ &\qquad + \int_{(m-2)T_\mathrm{s}}^{(m-1)T_\mathrm{s}} n(t) e^{-\jmath 2\pi \frac{t}{T_\mathrm{s}}} \mathrm{d}t \\ &= \dot{G}_{1,m} + n_{1,m}. \\ G_{2,m} &= \int_{(m-2)T_\mathrm{s}}^{(m-1)T_\mathrm{s}} r_m(t) e^{-\jmath 4\pi \frac{t-(m-2)T_\mathrm{s}}{T_\mathrm{s}}} \mathrm{d}t \\ &= \underbrace{\eta_m T_\mathrm{s} A_{\mathrm{h},m}^2 e^{\jmath 2(\bar{\theta}_m - \omega_0\tau_m)}}_{\dot{G}_{2,i}} + \int_{(m-2)T_\mathrm{s}}^{(m-1)T_\mathrm{s}} n(t) e^{-\jmath 4\pi \frac{t}{T_\mathrm{s}}} \mathrm{d}t \\ &= \dot{G}_{2,m} + n_{2,m}, \end{aligned} \tag{29}$$

where $n_{k,m} = \int_{(m-2)T_\mathrm{s}}^{(m-1)T_\mathrm{s}} n(t) e^{-\jmath 2\pi k t/T_\mathrm{s}} \mathrm{d}t$ and the overhead dot denotes the noise-free component. Since the basis functions $\exp(-\jmath 2\pi k t/T_\mathrm{s}), k = 0, 1, 2$ in (27)-(29) are orthogonal and have equal energy, the noise terms $n_{0,m}$, $n_{1,m}$, $n_{2,m}$ are independent and have equal variance $\sigma_n^2 = T_\mathrm{s} N_0$. Hence, for each of the integration outputs, we can define individual SNRs

$$\gamma_{0,m} = \frac{|\dot{G}_{0,m}|^2}{\sigma_n^2} = \frac{\eta_m^2 A_{\mathrm{p},m-1}^4 T_\mathrm{s}}{N_0}, \tag{30}$$

$$\gamma_{1,m} = \frac{|\dot{G}_{1,m}|^2}{\sigma_n^2} = \frac{4\eta_m^2 A_{\mathrm{h},m}^2 A_{\mathrm{p},m-1}^2 T_\mathrm{s}}{N_0}, \tag{31}$$

$$\gamma_{2,m} = \frac{|\dot{G}_{2,m}|^2}{\sigma_n^2} = \frac{\eta_m^2 A_{\mathrm{h},m}^4 T_\mathrm{s}}{N_0}. \tag{32}$$

Given (27)-(29), helper m can estimate the phase offset $\varphi_{\mathrm{o},m}$ as

$$\hat{\varphi}_{\mathrm{o},m} = \arg(G_{0,m} G_{1,m}^*), \tag{33}$$

where $(\cdot)^*$ denotes complex conjugate. Note that while we do not directly use the output $G_{2,m}$ of the third integrator for phase estimation, we will see in the following that it provides a useful SNR reference that is independent of the variable partial set amplitude $A_{\mathrm{p},m-1}$.

Phase estimation in (33) is similar to a phase error detection in a phase-locked loop. In contrast to operating directly on the magnitude of received measurements, it first projects the received signal onto a set of orthogonal subspaces and then extracts the phase. This separates the individual signal components and, by averaging over the sweep time, reduces the effect of additive noise.

V. Phase Adjustment Accuracy

Above, we presented a transmission scheme and a phase estimation method to phase-align helper node signals for coherent signal combining at the tag. In the absence of noise, it achieves phase alignment in $M-1$ slots. When an additive noise is present, how well the phases can be aligned depends on the phase estimation accuracy of (33). The following section presents an analysis of the phase adjustment accuracy of the

proposed approach and its effect on the REF of the helper-based system.

A. Phase Estimation

As a first step, we introduce a more compact notation. We normalize the helper amplitudes $A_{\mathrm{h},m}$ and partial helper set amplitudes $A_{\mathrm{p},m}$ by the RN amplitude A_{r} to obtain amplitude ratios $\alpha_m = A_{\mathrm{p},m}/A_{\mathrm{r}}$ and $\beta_m = A_{\mathrm{h},m}/A_{\mathrm{r}}$, and normalize the downlink gains η_m by the RN gain η_{r} to obtain the downlink ratios $\eta'_m = \eta_m/\eta_{\mathrm{r}}$. All three ratios are unitless. With these, we can relate all SNRs to that of the RN which is given by

$$\gamma_{\mathrm{r}} = \frac{\eta_{\mathrm{r}}^2 A_{\mathrm{r}}^2 T_{\mathrm{s}}}{N_0}. \tag{34}$$

Thus, using (30)–(32) in reverse order we obtain

$$\gamma_{2,m} = \frac{\eta_m^2 A_{\mathrm{r}}^4 \beta_m^4 T_{\mathrm{s}}}{N_0} = \eta_m'^2 \beta_m^4 \gamma_{\mathrm{r}}, \tag{35}$$

$$\gamma_{1,m} = \frac{4\, A_{\mathrm{p},m-1}^2}{A_{\mathrm{h},m}^2}\gamma_{2,m} = 4\eta_m'^2 \alpha_{m-1}^2 \beta_m^2 \gamma_{\mathrm{r}}, \tag{36}$$

$$\gamma_{0,m} = \frac{A_{\mathrm{p},m-1}^4}{A_{\mathrm{h},m}^4}\gamma_{2,m} = \eta_m'^2 \alpha_{m-1}^4 \gamma_{\mathrm{r}}. \tag{37}$$

Consider now (33) and rewrite $G_{0,m}$, $G_{1,m}$ in terms of $\gamma_{0,m}, \gamma_{1,m}$ so that

$$G_{0,m} G_{1,m}^* = \sigma_n^2 \sqrt{\gamma_{0,m}\gamma_{1,m}} e^{\jmath \varphi_{\mathrm{o},m}} + n_{\mathrm{t},m}, \tag{38}$$

where

$$n_{\mathrm{t},m} = \sigma_n \left(\sqrt{\gamma_{1,m}} e^{-\jmath \arg(\dot{G}_{1,m})} n_{0,m} + \sqrt{\gamma_{0,m}} e^{-\jmath \arg(\dot{G}_{0,m})} n_{1,m}\right) + n_{0,m} n_{1,m}^*. \tag{39}$$

From (38), the phase offset $\varphi_{\mathrm{o},m}$ can be written as

$$\hat{\varphi}_{\mathrm{o},m} = \arg(G_{0,m} G_{1,m}^*) = \varphi_{\mathrm{o},m} + \varphi_{\mathrm{er},m}, \tag{40}$$

where $\varphi_{\mathrm{er},m}$ is the noise-induced phase estimation error suffered by helper m in phase adjustment slot $i = m-1$. As a result, even if the partial set amplitude $A_{\mathrm{p},m-1}$ and helper-m amplitude are known before the adjustment, the post-adjustment partial set amplitude $A_{\mathrm{p},m}$ is a random variable.

The three terms that constitute $n_{\mathrm{t},m}$ in (39) are uncorrelated, so its variance is

$$\sigma_m^2 = (\gamma_{0,m} + \gamma_{1,m} + 1)\, \sigma_n^4. \tag{41}$$

Because of the quadratic term $n_{0,m} n_{1,m}^*$ the noise $n_{\mathrm{t},m}$ is not strictly Gaussian. Nevertheless, when its two linear components dominate the quadratic term ($\gamma_{0,m} + \gamma_{1,m} \geq 1$), $n_{\mathrm{t},m}$ can be well approximated as zero-mean complex Gaussian. In this case, $G_{0,m} G_{1,m}^*$ has a non-central complex Gaussian distribution with a K-factor (ratio of the squared mean to the variance, another SNR measure) equal to

$$K_m \triangleq \frac{\left(\sigma_n^2 \sqrt{\gamma_{0,m}\gamma_{1,m}}\right)^2}{(\gamma_{0,m} + \gamma_{1,m} + 1)\, \sigma_n^4} = \frac{\gamma_{0,m}\gamma_{1,m}}{\gamma_{0,m} + \gamma_{1,m} + 1}. \tag{42}$$

Substituting (36), (37) into (42), the K-factor becomes

$$K_m = \frac{4\alpha_{m-1}^6 \gamma_{2,m}^2}{\alpha_{m-1}^4 \beta_m^2 \gamma_{2,m} + 4\alpha_{m-1}^2 \beta_m^4 \gamma_{2,m} + \beta_m^6} = \frac{4\eta_m'^4 \alpha_{m-1}^6 \beta_m^2 \gamma_{\mathrm{r}}^2}{\eta_m'^2 \alpha_{m-1}^4 \gamma_{\mathrm{r}} + 4\eta_m'^2 \alpha_{m-1}^2 \beta_m^2 \gamma_{\mathrm{r}} + 1}. \tag{43}$$

As for the phase error $\varphi_{\mathrm{er},m}$, its distribution is that of the phase of (38) when $\varphi_{\mathrm{o},m} = 0$. From [34, eq. (5.33)], its PDF is

$$f_{\varphi_{\mathrm{er},m}}(\varphi_{\mathrm{er},m}, K_m) = \frac{e^{-K_m}}{2\pi}\left(1 + \sqrt{4\pi K_m} z_m e^{K_m x^2} Q(-\sqrt{2K_m} z_m)\right), \tag{44}$$

where $z_m = \cos\varphi_{\mathrm{er},m}$ and $Q(\cdot)$ denotes the complementary cumulative distribution function (CCDF) of a standard Gaussian distribution.

B. Phase Adjustment

Consider now the phase adjustment process exemplified by Frame 1 in Fig. 4. Our primary interest is how the partial helper set amplitude $A_{\mathrm{p},m}$ changes from slot to slot as each additional helper adjusts its phase. Since helper 1 does not adjust its phase, the process is initialized with $A_{\mathrm{p},1} = A_{\mathrm{h},1}$ or, equivalently, with $\alpha_1 = \beta_1$. In the first slot, helper 2 tries to align its phase with that of helper 1. Elementary geometry gives post-adjustment amplitude for use in the next slot as

$$A_{\mathrm{p},2} = \sqrt{A_{\mathrm{h},2}^2 + 2A_{\mathrm{p},1}A_{\mathrm{h},2}\cos\varphi_{\mathrm{er},2} + A_{\mathrm{p},1}^2}, \tag{45}$$

and substitution of the normalized amplitudes α_2 and β_2 gives the equivalent expression

$$\alpha_2 = \sqrt{\beta_2^2 + \alpha_1\beta_2\cos\varphi_{\mathrm{er},2} + \alpha_1^2}. \tag{46}$$

Generalizing to adjustment of helper m in slot $m-1$, we have the new partial set amplitude ratio for slot m as

$$\alpha_m = \sqrt{\beta_m^2 + 2\alpha_{m-1}\beta_m\cos(\varphi_{\mathrm{er},m}) + \alpha_{m-1}^2}, \tag{47}$$

in which $\alpha_m \in [\max(\alpha_{m-1} - \beta_m, 0), \alpha_{m-1} + \beta_m]$ for any $2 \leq m \leq M$.

From (47), the amplitude ratio α_m for $m \geq 2$ is a random variable that depends both on the phase estimation error in the current slot $\varphi_{\mathrm{er},m}$ and the amplitude ratio in the previous slot α_{m-1}. Next, we obtain its conditional PDF $f_{\alpha_m}(\alpha_m|\alpha_{m-1})$. Define $z_m = \cos\varphi_{\mathrm{er},m}$ and express $\varphi_{\mathrm{er},m}$ in terms of z_m. From (47) it is equivalent to

$$\varphi_{\mathrm{er},m} = \arccos z_m = \arccos\left(\frac{\alpha_m^2 - \alpha_{m-1}^2 - \beta_m}{2\alpha_{m-1}\beta_m}\right). \tag{48}$$

Note that (48) is symmetric about zero as is the PDF (44), so there are two mirror-image branches to consider. For convenience, we take the positive branch and multiply the result by 2. Applying the change of variables, we obtain

$$f_{\alpha_m}(\alpha_m|\alpha_{m-1}) = -2 f_{\varphi_{\mathrm{er},m}}(\varphi_{\mathrm{er},m}, K_m)\frac{\mathrm{d}\varphi_{\mathrm{er},m}}{\mathrm{d}\alpha_m}, \tag{49}$$

in which

$$\frac{\mathrm{d}\varphi_{\mathrm{er},m}}{\mathrm{d}\alpha_m} = -\frac{\alpha_m}{\beta_m\alpha_{m-1}}\frac{1}{\sqrt{1-\left(\frac{\alpha_m^2-\alpha_{m-1}^2-\beta_m}{2\alpha_{m-1}\beta_m}\right)^2}} = -\frac{\alpha_m}{\beta_m\alpha_{m-1}}\frac{1}{\sqrt{1-z_m}}. \quad (50)$$

Combining (50) with (49) we have the conditional PDF

$$f_{\alpha_m}(\alpha_m|\alpha_{m-1}) = \frac{e^{-K_m}}{\pi}\frac{\alpha_m}{\beta_m\alpha_{m-1}}\frac{1}{\sqrt{1-z_m^2}} \quad (51)$$

$$\times\left(1+\sqrt{4\pi K_m}z_m e^{K_m z_m^2}Q(-\sqrt{2K_m}z_m)\right), \quad (52)$$

where $z_m = (\alpha_m^2 - \alpha_{m-1}^2 - \beta_m)/2\alpha_{m-1}\beta_m$.

The unconditional PDF $f_{\alpha_m}(\alpha_m)$ is obtained by marginalizing (52) over the distribution of α_{m-1}:

$$f_{\alpha_m}(\alpha_m) = \int_0^{u_m} f(\alpha_m|\alpha_{m-1})f(\alpha_{m-1})\mathrm{d}\alpha_{m-1}, \quad (53)$$

where $u_m = \sum_{k-1}^{m}\beta_k$. For $m = 2$, where $\alpha_1 = \beta_1$ in K_2 and z_2, (53) has a closed-form solution which is given by

$$f_{\alpha_2}(\alpha_2) = \frac{e^{-K_2}}{\pi}\frac{\alpha_2}{\beta_2\beta_1}\sqrt{\frac{1}{1-z_2^2}}\left(1+\sqrt{\pi K_2}z_2 e^{K_2 x_2^2}Q(-\sqrt{2K_2}z_2)\right). \quad (54)$$

For any $2 < m \leq M$, the unconditional PDF $f_{\alpha_m}(\alpha_m)$ can then be obtained numerically by successive iterations of the recursion (53).

To illustrate the successive PDFs over the $M-1$ adjustment slots, we start with a simplified scenario in which all downlink factors η_m are equal and all helper amplitudes are equal to the amplitude of the RN, $\beta_m = 1$ for $m = 1, \ldots, M$ (hence $\alpha_1 = 1$). The SNRs $\gamma_{2,m}, m = 1, \ldots, M$ are then all equal and denoted simply by γ_2. Fig. 5 exhibits PDFs of the partial helper set amplitudes, adjustment after adjustment, for different values of m and input SNR γ_2 ranging from -5 to 5 dB. In Fig. 5(a), we observe that the theoretical PDFs computed via (54) coincide well with the empirical ones for both considered SNRs. Fig. 5(b) on the other hand, illustrates that, as the phase adjustment proceeds from slot to slot and the number of helpers m grows, so does the likelihood that the partial set amplitude $A_{\mathrm{p},m}$ increases, as higher values of the amplitude ratio in previous slots lead to improved phase estimation performance (via increased K-factor) and thus better chances for obtaining higher amplitude ratio and higher SNR in the current slot. Further, the long-tailed asymmetry of the PDFs shows that, while $A_{\mathrm{p},m}$ is almost always close to mA_{r}, it can fall to very low values on rare occasions. Therefore, our design analysis should be based on performance percentiles, rather than on the average values.

In Fig. 6 we examine a more ambitious scenario: differing amplitudes among $M = 4$ helpers. It shows the cumulative distribution functions (CDFs) of the amplitude ratio α_M after final, $(M-1)$-th, phase adjustment for three cases characterized by the following values of β_m: largest first $\{1.323, 1.118, 0.866, 0.5\}$, smallest first $\{0.5, 0.866, 1.118, 1.323\}$, and equal $\{1, 1, 1, 1\}$. These values are selected so that $\sum_m \beta_m^2 = M$ resulting in the sum of individual helper powers at the tag being the same for all cases. For simplicity, downlink factors are made equal ($\eta'_m = 1$ for all m). The reference SNR is $\gamma_{\mathrm{r}} = -5$ dB, so (36) gives the individual SNRs as: largest first $\{-0.138, -3.06, -7.45, -17.0\}$ dB, smallest first $\{-17.0, -7.45, -3.06, -0.138\}$ dB, and for equal powers,

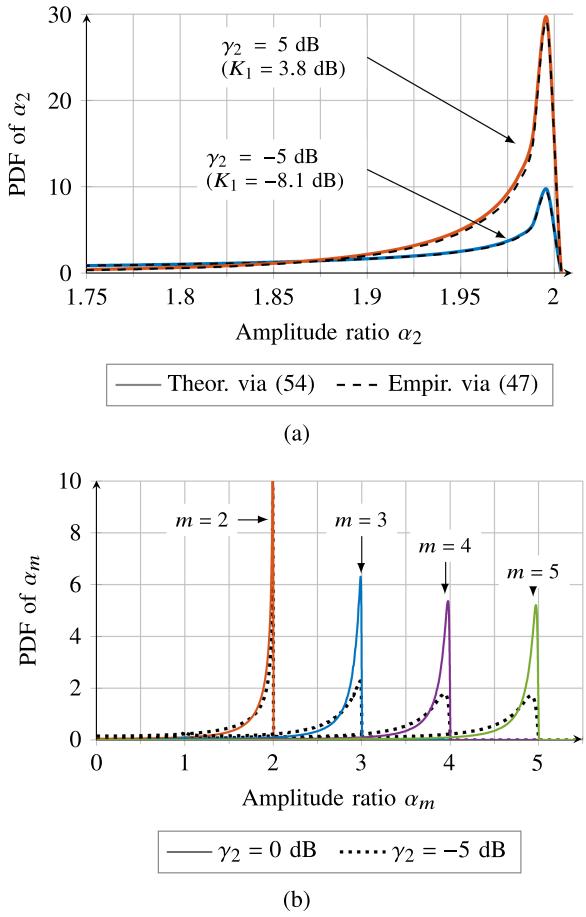

Fig. 5. Exemplary PDFs of the amplitude ratio α_m for (a) $m = 2$ and (b) $m \in [2, 5]$ when $\beta_m = 1$ and $\eta_m = \eta_{\mathrm{r}}$ for all $m \in [1, M]$.

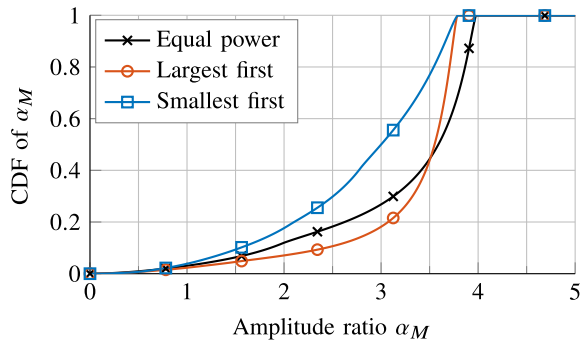

Fig. 6. CDFs of the amplitude ratio α_M for $M = 4$ helpers with differing amplitudes for three cases: $\beta_m = 1$ for all m (equal power), $\{\beta_m\} = \{1.323, 1.118, 0.866, 0.5\}$ (largest first), and $\{\beta_m\} = \{0.5, 0.866, 1.118, 1.323\}$ (smallest first).

all are -5 dB. These poor SNRs are intended to highlight relevant phenomena in statistics of α_M. Fig. 6 shows that both smallest first and largest first have the same maximum possible helper sum ($3.8 = \sum_{m=1}^{M} \beta_m$), but largest first generally provides a better performance. Equal power has a larger maximum possible value ($\sum_{m=1}^{M} \beta_m = M = 4$). However, its CDF crosses that of the largest first at 3.5 at probability 0.438. That is, equal power has a higher probability of small amplitudes than largest first, even though it is preferable to largest first at high amplitudes. This reinforces the need for design to be based on performance percentiles.

There are many other parameter variations to explore, and the differences among downlink gains expands that space further. We have provided the analytical tools for such investigations. However, given the space limitations of the present paper, the analytical and numerical explorations to follow will adopt the simplified scenario of Fig. 5 in which all normalized downlink factors η'_m and helper amplitudes β_m are equal to one and the SNRs $\gamma_{2,m} = \gamma_2 = \gamma_\mathrm{r}$ for all m.

C. Effect on Ranging SNR and REF

Now we demonstrate the range extension provided by our helper-based system and compare it to the range extension achievable by a conventional system that is given the same total transmit power. The helper-based HR system uses the intermodulation term (the second term of (13)) for ranging. Previously, we saw that its instantaneous power is

$$P_\mathrm{i} = 4A_\mathrm{h}^2 A_\mathrm{r}^2 \le 4A_\mathrm{r}^2 \left(\sum_{m=1}^{M} A_{\mathrm{h},m} \right)^2 = 4A_\mathrm{r}^4 \sum_{m=1}^{M} \beta_m^2, \quad (55)$$

with the upper limit being achieved when all M helper tones perfectly phase-align at the tag. After the last, $(M-1)$-th, phase adjustment slot, the helper node amplitude becomes $A_\mathrm{h} = A_{\mathrm{p},M-1}$ and (55) can be written as

$$P_\mathrm{i} = 4\alpha_M^2 A_\mathrm{r}^4, \quad (56)$$

where $\alpha_M = A_\mathrm{h}/A_\mathrm{r}$. Comparing (56) with the power of the ranging term (term 1 in (13)), we see that the SNR boost is proportional to $4\alpha_M^2$ while the corresponding REF for phase adjustment is then $\zeta_\mathrm{pa} = \sqrt[3]{2\alpha_M}$. With another change of variable, we obtain the PDF of ζ_pa as

$$f_{\zeta_\mathrm{pa}}(\zeta_\mathrm{pa}) = 1.5\zeta_\mathrm{pa}^2 f_{\alpha_M}(\zeta_\mathrm{pa}). \quad (57)$$

Its CDF is $F_{\zeta_\mathrm{pa}}(\zeta_\mathrm{pa}) = \int_0^{\zeta_\mathrm{pa}} f_{\zeta_\mathrm{pa}}(\zeta_\mathrm{pa})\mathrm{d}\zeta_\mathrm{pa}$. We also define the inverse function of the CDF as

$$G_{\zeta_\mathrm{pa}}(p) \triangleq \zeta_\mathrm{pa} : F_{\zeta_\mathrm{pa}}(\zeta_\mathrm{pa}) = 0.01p. \quad (58)$$

That is, $G_{\zeta_\mathrm{pa}}(p)$ is the value of the REF ζ_pa at the p-th percentile.

We evaluate the REF on an example of a simplified scenario in which $\eta_m = \eta_\mathrm{r}$ and $\beta_m = 1$ for all $m = 1, \ldots, M$. Fig. 7 depicts $G_{\zeta_\mathrm{pa}}(p)$ as a function of M for input SNR $\gamma_2 = -5$ dB. It shows a conservative 10th percentile as a worst acceptable case, as well as the more optimistic 50th percentile along with the corresponding REFs of a brute-force conventional HR system

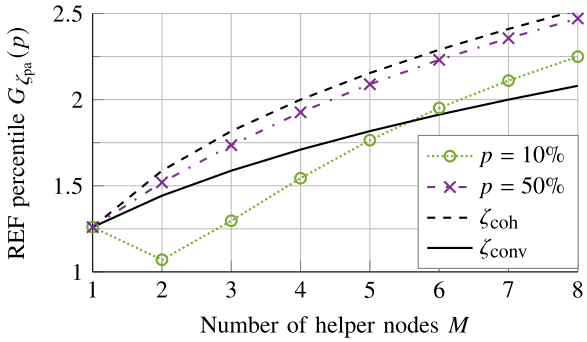

Fig. 7. REF percentiles as a function of M for input SNR $\gamma_2 = -5$ dB when $\beta_m = 1$ and $\eta_m = \eta_\mathrm{r}$ for all $m \in [1, M]$. The solid black line indicates REF of the conventional brute-force HR system without helper nodes $\zeta_\mathrm{conv} = \sqrt[3]{M+1}$ (22) while the black dashed line shows REF of a fully coherent helper-based system $\zeta_\mathrm{coh} = \sqrt[3]{2\,M}$ (17).

$\zeta_\mathrm{conv} = \sqrt[3]{M+1}$ (22) and a fully coherent helper-based system $\zeta_\mathrm{coh} = \sqrt[3]{2\,M}$ (17). All three systems have the same total EIRP. We observe from Fig. 7 that, at this SNR ($\gamma_2 = -5$ dB), one could expect a range extension factor greater than one ($\zeta_\mathrm{pa} > 1$) even in the worst-case scenario[4], while in 50% of cases the REF of the helper-based system well exceeds that of the conventional brute-force approach when both systems are given the same total transmission power.

D. Slot Duration Limitations

In our helper-based system, the phase adjustment interval consists of $M-1$ slots followed by a ranging interval. Each phase adjustment slot lasts T_s seconds during which the A-mode helper sweeps its phase according to the sweep function $\varphi(t) = 2\pi t/T_\mathrm{s}$ and collects the tag response in order to compute its phase correction according to (33). While it appears that the slot duration T_s is a free parameter of choice, there are several considerations that limit its practical range.

The i-th phase adjustment slot ($i > 1$) is launched with the helper node phases of nodes 1 to i obtained by the end of the preceding slot. The primary concern then is the phase drift due to frequency errors in LOs of the helpers and, if they or the tag are moving, differences in their Doppler shifts. Phase drift causes increasing de-coherence among helpers across the slot time, with a corresponding slow reduction of the amplitude ratio α_i through the shrinking of the $A_{\mathrm{p},i}$ factor. Suppose that due to LO and movement-induced frequency shifts the k-th helper signal arriving at the tag has a frequency error $\omega_{\mathrm{er},k}$ at the end of the phase adjustment slot T_s, which causes a growing phase difference between the different helper tones. The longer the slot duration, the greater the phase difference. Since the phase difference must be contained over all $M-1$ phase adjustment

[4] At lower SNRs the long tails of $f_{\alpha_M}(\alpha_M)$ can cause the 10th percentile REF for $M > 1$ to fall below that of the constant REF provided by a single helper, which we observe in Fig. 7 for $M = 2$. Nevertheless, adding more helpers consistently improves the 10th percentile performance.

TABLE I
PARAMETERS OF A HR SYSTEM REPORTED IN [18]

Parameter	Value
Frequency $f_0/2f_0$	9.3/18.6 GHz
Receiver bandwidth B_r	125 kHz
Output power P_r	10 Watt
Tx/Rx antenna gain $G_\mathrm{tx} = G_\mathrm{rx}$	15 dBi
Rx noise figure N_F	2.5 dB

TABLE II
PARAMETERS OF A SCHOTTKY DIODE SMS7630-040 [35]

Parameter	Value
Saturation current I_s	5 μA
Ideality parameter n_i	1.05
Thermal voltage V_T	26 mV
Coefficient ρ	0.024

slots, we require that

$$T_\mathrm{s} \leq \frac{\Delta\theta_\mathrm{max}}{(M-1)\omega_\mathrm{er,max}}, \tag{59}$$

where $\Delta\theta_\mathrm{max}$ is the maximum allowable phase difference and $\omega_\mathrm{er,max}$ is the maximum frequency error of each helper.

According to (59), the phase drift limits the slot duration from above. However, the slot duration cannot be too brief either. Since the SNR $\gamma_{2,i}$ is proportional to T_s, it sets a minimum value for slot duration T_s required for reliable phase estimation so that

$$T_\mathrm{s} \geq \frac{\gamma_\mathrm{2,min} N_0}{P_\mathrm{h,min}}, \tag{60}$$

where $\gamma_\mathrm{2,min}$ is the minimum allowable input SNR for a desired performance level, while $P_\mathrm{h,min}$ indicates the minimum individual incident helper-tone power received by any A-mode node. In addition, because of the time it takes the signal from the A-mode helper to reach the tag, the phase offset that maximizes the helper node sum at the tag differs from the estimated one by $\theta_\mathrm{d} = 2\pi\tau_k/T_\mathrm{s}$. Clearly, when $\tau_k \ll T_\mathrm{s}$ the phase delay θ_d is negligible, which is why it was omitted earlier. Nevertheless, it contributes to the total phase difference and has to be accounted for when setting the SNR limit in (60).

Finally, combining (59) and (60) we arrive at

$$\frac{\gamma_\mathrm{2,min} N_0}{P_\mathrm{h,max}} \leq T_\mathrm{s} \leq \frac{\Delta\theta_\mathrm{max}}{(M-1)\omega_\mathrm{er,max}}, \tag{61}$$

which shows how the combination of noise, mobility and the number of helpers bounds the slot duration T_s. In the following, we explore (61) in more detail.

VI. NUMERICAL EXAMPLE

A. System Parameters

In this section, we numerically evaluate proposed HR system with adaptive self-coherent auxiliary helper nodes and compare it against conventional HR without helpers. As a benchmark, we consider an X-band HR system reported in [18] with operational parameters summarised in Table I. With an output transmit power of $P_\mathrm{r} = 10$ Watt and Tx/Rx antenna gains of 15 dBi, its reported maximum detection range is 15 m.

For modelling the behaviour of the harmonic tag, we consider a wire-based tag design from [17], [21] where the tag consists of a single dipole antenna that acts both as the receive antenna at ω_0 and the transmit antenna at $2\omega_0$, a Schottky diode and a parallel inductive loop. In our evaluation we use a Skyworks Schottky diode SMS7630-040 [35] with parameters specified in Table II. For simplicity, we also assume perfect matching conditions at both ω_0 and $2\omega_0$ such that $k_\mathrm{in} = k_\mathrm{out} = 1$. To facilitate this, we assume that the tag antenna is a half-wavelength dipole at ω_0 with an arm ratio of $(2:1)$, which, as outlined in [36], [37], ensures a double resonant structure necessary to maximise the power transfer efficiency of the tag. Using an antenna-analysis tool MMANA-GAL [38], we find that for a copper wire with a diameter of 0.31 mm this yields $|Z_\mathrm{F}| \approx R_\mathrm{F} = 132\,\Omega$, $|Z_\mathrm{H}| \approx R_\mathrm{H} = 146\Omega$, $G_\mathrm{tag}(\omega_0) = 2.2$dBi, $G_\mathrm{tag}(2\omega_0) = 3.15$ dBi. The tag antenna gains, together with the parameters from Table I, determine the uplink gain $h_\mathrm{u}(d)$ (2) and the downlink gain $h_\mathrm{d}(d)$ (8).

Given an arbitrary transmit waveform $x(t)$, a transmit power P_r and a downlink gain $h_\mathrm{d}(d)$, we can determine the input voltage at the tag antenna $v_\mathrm{in}(t)$ according to (2). Throughout this paper, we made use of the quadratic small-signal approximation (5) to model the relation between the input voltage $v_\mathrm{in}(t)$ at the tag and the tag output current at the second harmonic $i_2(t)$. Here, we employ the more general explicit solution to (4) instead [29]:

$$\tilde{i}_\mathrm{T}(t) = \left(\frac{W_0\left(\rho e^{(\rho + \tilde{v}_\mathrm{in}(t)/n_\mathrm{i} V_\mathrm{T})}\right)}{\rho} - 1 \right) I_\mathrm{S}, \tag{62}$$

in which $W_0(\cdot)$ denotes the principal branch of the Lambert function [39]. Given (62), we compute $i_2(t)$ numerically as

$$i_2(t) = a_2(t) - jb_2(t), \tag{63}$$

where $a_2(t), b_2(t)$ are the second harmonic Fourier coefficients of $\tilde{i}_\mathrm{T}(t)$ (see [29] for details). As before, the output tag voltage is

$$v_\mathrm{out} = |Z_\mathrm{H}| i_2(t). \tag{64}$$

Using (62) allows us to test how well our quadratic model holds and evaluate how the proposed algorithm behaves outside the quadratic region.

B. Conventional HR System

We begin our study by determining operational conditions of a conventional X-band HR system without helper nodes with parameters specified in Table I. Fig. 8 shows input signal power at the tag antenna, $P_\mathrm{in} = h_\mathrm{u}^2(d) P_\mathrm{r}$, and at the harmonic radar receiver, $P_\mathrm{rec} = h_\mathrm{d}^2(d) R_\mathrm{H} I_2^2/2$, for a tone input, where I_2 denotes the amplitude of the second harmonic current. We can clearly observe the change in the curve slope of P_rec appearing around $d = 4$m. It illustrates the transition from the quasi-linear regime characteristic of the large-signal conditions to the quadratic

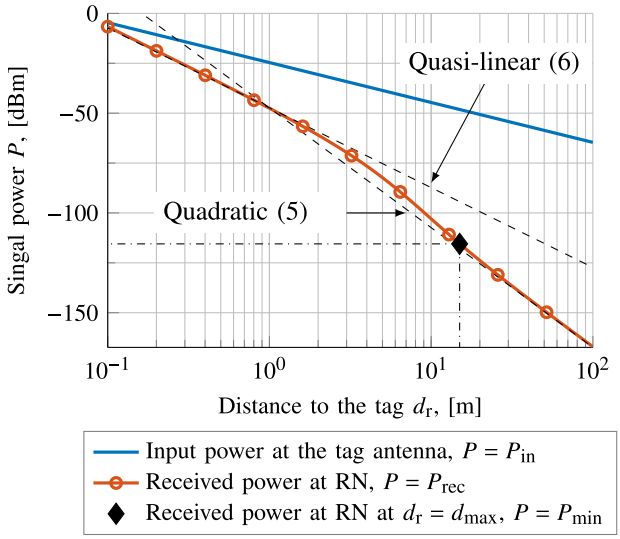

Fig. 8. Signal power as a function of the distance to the tag d_r in a conventional HR system without auxiliary helper nodes.

regime in the small-signal region. We also indicate here the point corresponding to the reported maximum detection range $d_{\max} = 15$ m [18], which is clearly in the quadratic region. It determines the minimum received signal power of $P_{\min} = -115.5$ dBm with a corresponding tag input power of $P_{\text{in}} = -48$ dBm. From this, we also compute a minimum required voltage amplitude at the tag, which is $A_r = 2.43 n_i V_T = 63$ mV. Finally, we determine the receiver noise power as $P_n = 2B_r N_0 \approx -118$ dBm, in which $N_0 = R_{rx} k_B T_n (N_f - 1)$ where $T_n = 290$ K is the standard room temperature and N_f is the Rx noise figure in linear scale.

C. HR System With Auxiliary Helper Nodes

This section examines the benefits of introducing helpers into the operational scenario described above. In what follows, we assume helper tones to arrive at the tag with the same amplitude, which is equal to RN amplitude ($A_{h,m} = A_r$ and $\beta_m = 1$ for any $m \in [1, M]$). In this case, when the helpers are perfectly phase-aligned at the tag the composite helper node amplitude A_h is equal to MA_r and the amplitude ratio at the end of the phase adjustment interval is $\alpha_M = M$.

First, we present the statistical distributions of the normalized amplitude ratio $\tilde{\alpha}_M = \alpha_M / M \in [0, 1]$. Previously, we saw that $f_{\alpha_M}(\alpha_M)$ depends on the input SNR[5] γ_2, which in turn depends both on the phase adjustment slot duration T_s via the integration time in (29) and the distance to the tag d_r via the amplitude of the receiver input. Suppose now that the tag is positioned at the maximum range of the conventional system such that $d_r = d_{\max}$. Then, the amplitude A_r is fixed and γ_2 is determined by the slot duration T_s. Fig. 9(a) shows 10th and 50th percentiles $G_{\tilde{\alpha}_M}(p)$ of the normalized amplitude ratio $\tilde{\alpha}_M$ as a function of the input SNR γ_2, together with the values of T_s corresponding to the SNRs. We observe good correspondence between the empirical results obtained using (62) and the theoretical ones derived from the asymptotic quadratic model (5). Fig. 9(a) also demonstrates that the phase adjustment performance improves both with M and the input SNR. For instance, when $M = 2$ and the slot duration is greater than one microsecond (i.e., $\gamma_2 > 0$), 90% of the outcomes achieve more than 60% of the maximum possible amplitude amplification (i.e., α_M is greater than $0.6M = 1.2$) while for $M = 4$ it exceeds 85% (i.e, α_M is greater than $0.85M = 3.4$). To test how well our approach performs outside of the quadratic region, we fix the slot duration T_s and change the distance to the tag d_r instead. Note that the slot duration is set to $T_s = 1$ns, an extremely low value, solely to avoid excessively large SNR values when the distance is small and the tag operates far above the quadratic region. Fig. 9(b) demonstrates the results. It indicates that the move towards the quasi-linear ($d_r << d_{\max}$) region does not significantly affect the ability of our phase adaptation algorithm to phase-align helper signals at the tag.

Next, we return to Section V-D considerations and determine the upper and lower bounds on slot duration that allow the helper-based HR system to outperform conventional HR, when both systems are given the same total transmit power budget. To this end, we again consider system performance at the maximum range by setting the tag distance to $d_{\max}$, as it is our primary region of interest. First, we study the lower bound (60) on slot duration T_s. To account for the propagation delay in the sweep function $\varphi(t)$, we introduce an additional error $\theta_d = 2\pi d_{\max}/cT_s$ into the phase offset estimate (40). As our performance metric we choose the amplitude of the helper-based system measured by the pessimistic 10th percentile point, i.e., $G_{2\alpha_M}(10)$. Recall that the amplitude of the signal into the tag is proportional to $2\alpha_M$ for helper-assisted HR (56) and to $M + 1$ for conventional HR (21). Thus, Fig. 9(a) shows the minimum slot duration required for that 10th percentile amplitude to exceed the conventional HR amplitude, i.e., $G_{2\alpha_M}(10) > M + 1$. For comparison, we also show theoretical and empirical curves obtained under the initial assumption that $\theta_d = 0$. Fig. 9(a) suggests that a slot duration of about 1μs ensures that the SNR boost of the helper-node system exceeds that of a comparable conventional system in 90% of the cases. The slot duration can be further reduced by accepting a lower percentage of outcomes in which $2\alpha_M > M + 1$, e.g., by considering a 50th percentile instead.

We now turn to evaluating the upper bound (59) on slot duration T_s that still allows the pessimistic 10th amplitude percentile in helper-based HR to exceed the amplitude of the conventional HR. We introduce a frequency error ω_{er} as a portion of the fundamental carrier frequency ω_0, so that $\omega_{er}/\omega_0 = 10^{-6} p_e$ where p_e is the frequency instability expressed in parts per million (ppm). Given ω_{er}, the maximum phase error between any two helpers over the slot duration is $2\omega_{er} T_s$. Fig. 10(b) shows the maximum slot duration T_s that permits $G_{2\alpha_M}(10\%) > M + 1$ as a function of the number of helpers M, for two values of p_e. As expected, the upper bound begins to approach the lower one from Fig. 10(a) when the frequency error is increased. As

[5]In light of using (62) for determining the tag output, we define γ_2 here as the SNR at the output of the third integrator (29) during the first phase adjustment slot, i.e., $\gamma_2 = \gamma_{2,1} = |\dot{G}_{2,1}|^2 / T_s N_0$.

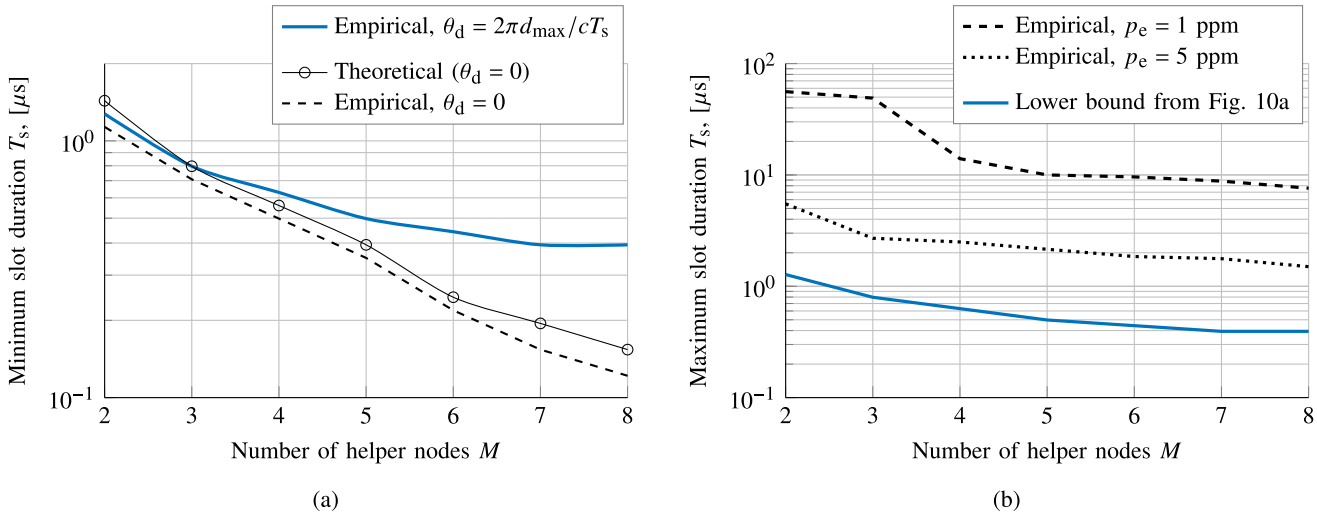

Fig. 9. Normalized amplitude ratio percentile $G_{\tilde{\alpha}_M}(p)$ as a function of the input SNR γ_2 (a) at a fixed distance $d_r = d_{max}$ and (b) at a fixed slot duration $T_s = 1$ns.

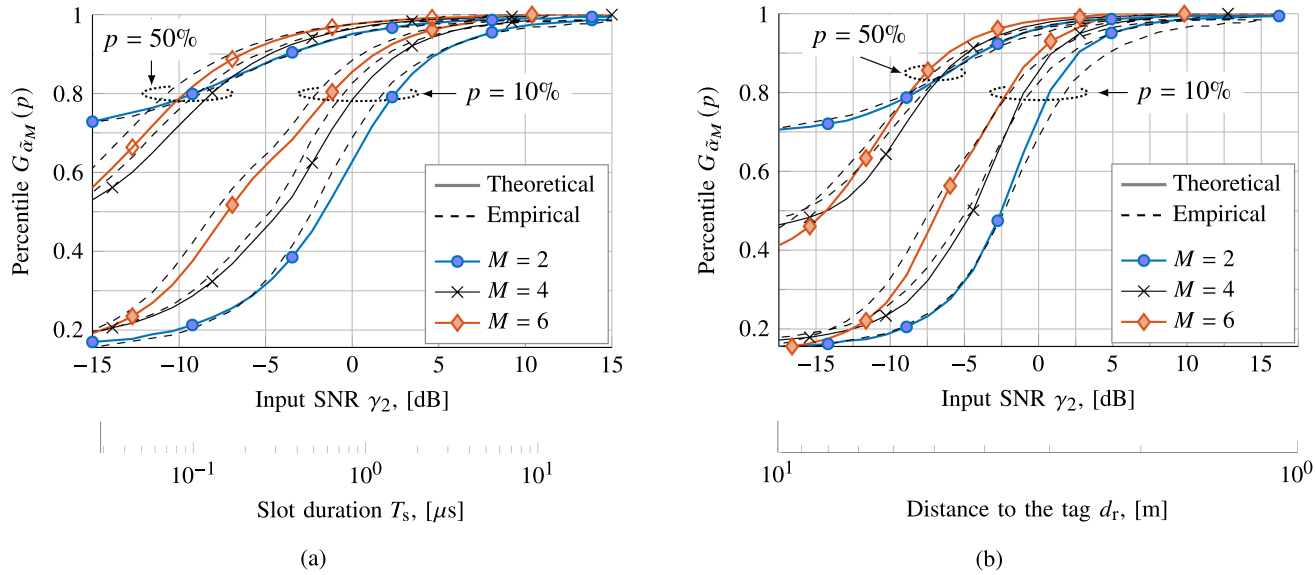

Fig. 10. Slot duration required for 10th percentile of helper-based HR amplitude $G_{2\alpha_M}(10)$ to exceed conventional HR amplitude $M+1$: (a) minimum required T_s in the presence of the propagation delay $\theta_d = 2\pi d_{max}/cT_s$ and (b) maximum allowed T_s in the presence of the frequency error $\omega_{err} = 10^{-6} p_e \omega_0$.

a result, for large enough frequency errors there might be no suitable slot duration that fulfills (61) for the performance metric of choice, so one would have to accept a higher probability of low-power outcomes. On the other hand, Fig. 10 shows that when the frequency error is within several ppm, the interplay between noise, frequency instability and the number of helpers provides enough room to choose T_s that ensures that the probability of low-power outcome does not exceed a desired value (10% in our case).

Our third, and final, assessment is to fix the slot duration and evaluate the REF of our phase-adaptive helper-based system ($\zeta_{pa} = \sqrt[3]{2\alpha_M}$) taking into account both the phase delay θ_d and the frequency error ω_{err}. Fig. 11 shows the CDF of ζ_{pa} for $T_s = 1\mu$s (i.e., $\gamma_2 = 0.4$dB at d_{max}) and $p_e = 1$ ppm. For comparison, it also provides corresponding values for the fully coherent system ($\zeta_{coh} = \sqrt[3]{2\,M}$, marked by circles) and the brute-force conventional system ($\zeta_{conv} = \sqrt[3]{M+1}$, marked by filled rhomboids). We observe that setting the slot duration within the limits determined by the performance bounds from Fig. 10 results in the phase-adaptive system outperforming the conventional HR with equivalent total transmit power with high probability, i.e., in more than 80% of the cases. Furthermore, the performance gap between the two increases with M. These results show that helpers can be added incrementally in order to achieve the desired range or SNR increase, as long as the system design satisfies (61).

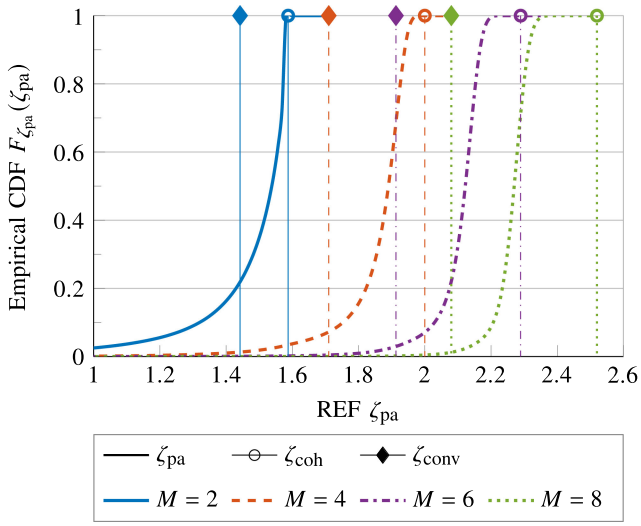

Fig. 11. CDFs of the REF $\zeta_{\rm pa}$ of the phase-adaptive helper-based system with the slot duration of 1μs and a frequency instability of 1 ppm. Individual circle and rhomboid markers show the corresponding REFs of a fully coherent helper-based system $\zeta_{\rm coh} = \sqrt[3]{2\,M}$ and a brute-force conventional system without helpers $\zeta_{\rm conv} = \sqrt[3]{M+1}$, respectively.

VII. Conclusion

The low power conversion efficiency of passive harmonic tags severely limits operational range in harmonic radar. The conventional remedy is ever-higher power at the uplink transmitter, but the inverse sixth power dependence on distance makes this an expensive method in HR. In contrast, our approach is based on new physical and signal configurations. Unconventionally, we use "helper nodes" to transmit tones that arrive as a single composite tone at the nonlinear tag while the ranging node transmits its own signal. The maximum benefit however, requires the helper tones to arrive coherently at the tag. Ensuring that condition was the focus of this paper.

Our phase-adaptation algorithm causes each helper, one at a time, to adjust its phase at the tag, aligning it with the composite tone from previously-aligned helpers based on the tag feedback. The adjusting helper sweeps its phase around the circle in the uplink while receiving the downlink signal. From a Fourier-like decomposition of the received signal, it estimates its required phase adjustment. Receiver noise causes adjustment error and consequent statistical variation in the composite helper sum at the tag. We provide analysis of the resulting distribution of the helper sum amplitude with a closed-form solution for $M = 2$ helpers and a recursion for $M > 2$. The result is a long-tailed distribution in which the 50th percentile is close to the maximum value, but the 10th percentile can be much lower, depending on the SNR and M. Assessment of the proposed method based on a measurement set from a prototype HR ranging node [18] showed that the proposed approach can be a viable solution for increasing detection range and/or SNR, or decreasing Tx/Rx antenna gains at RN, in HR-based systems.

In the pursuit of range increase, it may become an implementation issue whether our helper-based system or the conventional system is preferable. We note, however, that conventional ranging nodes become bigger, heavier and costlier as their transmit power increases, and they may require additional linearization. In contrast, the helper-based system can add power incrementally by adding nodes as needed, without requiring upgrades to the RN or any change to existing HNs or the high-level protocol to adjust their phases. Moreover, for systems with multiple RNs, a single set of helpers boosts the effective power of every RN. An alternative to increasing the range is to reduce the uplink and downlink antenna gains which can also provide savings in size and cost.

Our overall conclusion is that a helper-based system, relative to conventional harmonic radar systems, offers greater operational flexibility, as well as improved receiver sensitivity and higher power efficiency—and therefore the opportunity to increase the range, or reduce the required transmit power or antenna gains at the ranging node. The success of the helper-node structure prompts questions that should be addressed in further research. One issue is that powerful tones, as emitted from the helpers, are generally unwelcome near other electronics. Are there alternative helper signals that have a lower power spectral density, do not interfere with the ranging application and still allow easy separation of intermodulation components for estimate of phase errors, or other property? Another question is additional application areas. Could our adaptive phase coherence at a point in space be used for, say, backscatter communications?

References

[1] A. F. Martone, K. I. Ranney, K. D. Sherbondy, K. A. Gallagher, G. J. Mazzaro, and R. M. Narayanan, "An overview of spectrum sensing for harmonic radar," in *Proc. Int. Symp. Fundamentals Elect. Eng.*, 2016, pp. 1–5.

[2] X. Gu, N. N. Srinaga, L. Guo, S. Hemour, and K. Wu, "Diplexer-based fully passive harmonic transponder for sub-6-GHz 5G-compatible IoT applications," *IEEE Trans. Microw. Theory Techn.*, vol. 67, no. 5, pp. 1675–1687, May 2019.

[3] X. Hui and E. C. Kan, "Radio ranging with ultrahigh resolution using a harmonic radio-frequency identification system," *Nature Electron.*, vol. 2, no. 3, pp. 125–131, 2019.

[4] D. Kumar, S. Mondal, S. Karuppuswami, Y. Deng, and P. Chahal, "Harmonic RFID communication using conventional UHF system," *IEEE J. Radio Freq. Identif.*, vol. 3, no. 4, pp. 227–235, Dec. 2019.

[5] N. Nourshamsi, S. Vakalis, and J. A. Nanzer, "Joint detection of human and object motion using harmonic micro-doppler radar and harmonic tags," *IEEE Antennas Wireless Propag. Lett.*, vol. 19, no. 6, pp. 930–934, Jun. 2020.

[6] M. E. O'Neal, D. Landis, E. Rothwell, L. Kempel, and D. Reinhard, "Tracking insects with harmonic radar: A case study," *Amer. Entomologist*, vol. 50, no. 4, pp. 212–218, 2004.

[7] G. J. Mazzaro, A. F. Martone, K. I. Ranney, and R. M. Narayanan, "Nonlinear radar for finding RF electronics: System design and recent advancements," *IEEE Trans. Microw. Theory Techn.*, vol. 65, no. 5, pp. 1716–1726, May 2017.

[8] S. Mondal, D. Kumar, and P. Chahal, "Recent advances and applications of passive harmonic RFID systems: A review," *Micromachines*, vol. 12, no. 4, pp. 1–22, 2021.

[9] X. Gu, P. Burasa, S. Hemour, and K. Wu, "Recycling ambient RF energy: Far-field wireless power transfer and harmonic backscattering," *IEEE Microw. Mag.*, vol. 22, no. 9, pp. 60–78, Sep. 2021.

[10] B. Kubina, J. Romeu, C. Mandel, M. Schüßler, and R. Jakoby, "Quasi-chipless wireless temperature sensor based on harmonic radar," *Electron. Lett.*, vol. 50, no. 2, pp. 86–88, 2014.

[11] A. Lazaro, R. Villarino, and D. Girbau, "A passive harmonic tag for humidity sensing," *Int. J. Antennas Propag.*, vol. 2014, pp. 1–11, 2014.

[12] A. Singh and V. M. Lubecke, "Respiratory monitoring and clutter rejection using a CW doppler radar with passive RF tags," *IEEE Sensors J.*, vol. 12, no. 3, pp. 558–565, Mar. 2012.
[13] L. Chioukh, H. Boutayeb, D. Deslandes, and K. Wu, "Noise and sensitivity of harmonic radar architecture for remote sensing and detection of vital signs," *IEEE Trans. Microw. Theory Techn.*, vol. 62, no. 9, pp. 1847–1855, Sep. 2014.
[14] V. Palazzi *et al.*, "Demonstration of a chipless harmonic tag working as crack sensor for electronic sealing applications," *Wireless Power Transfer*, vol. 2, no. 2, pp. 78–85, 2015.
[15] A. Abdelnour, A. Lazaro, R. Villarino, D. Kaddour, S. Tedjini, and D. Girbau, "Passive harmonic RFID system for buried assets localization," *Sensors*, vol. 18, no. 11, 2018, Art. no. 3635.
[16] K. Rasilainen and V. V. Viikari, "Transponder designs for harmonic radar applications," *Int. J. Antennas Propag.*, vol. 2015, pp. 1–9, 2015.
[17] A. Lavrenko, B. Litchfield, G. Woodward, and S. Pawson, "Design and evaluation of a compact harmonic transponder for insect tracking," *IEEE Microw. Wireless Compon. Lett.*, vol. 30, no. 4, pp. 445–448, Apr. 2020.
[18] G. Storz and A. Lavrenko, "Compact low-cost FMCW harmonic radar for short range insect tracking," in *Proc. IEEE Int. Radar Conf.*, 2020, pp. 642–647.
[19] J. Riley and A. Smith, "Design considerations for an harmonic radar to investigate the flight of insects at low altitude," *Comput. Electron. Agriculture*, vol. 35, no. 2-3, pp. 151–169, 2002.
[20] D. Milanesio, M. Saccani, R. Maggiora, D. Laurino, and M. Porporato, "Design of an harmonic radar for the tracking of the Asian yellow-legged hornet," *Ecol. Evol.*, vol. 6, no. 7, pp. 2170–2178, 2016.
[21] B. G. Colpitts and G. Boiteau, "Harmonic radar transceiver design: Miniature tags for insect tracking," *IEEE Trans. Antennas Propag.*, vol. 52, no. 11, pp. 2825–2832, Nov. 2004.
[22] Z.-M. Tsai *et al.*, "A high-range-accuracy and high-sensitivity harmonic radar using pulse pseudorandom code for bee searching," *IEEE Trans. Microw. Theory Techn.*, vol. 61, no. 1, pp. 666–675, Jan. 2013.
[23] R. Maggiora, M. Saccani, D. Milanesio, and M. Porporato, "An innovative harmonic radar to track flying insects: The case of Vespa velutina," *Sci. Rep.*, vol. 9, no. 1, pp. 1–10, 2019.
[24] A. Lavrenko, S. Pawson, and J. Cavers, "On the use of additional transmitters for increasing detection range in harmonic radar," in *Proc. 13th Int. Conf. Signal Process. Commun. Syst.*, 2019, pp. 1–8.
[25] G. J. Mazzaro, A. F. Martone, and D. M. McNamara, "Detection of RF electronics by multitone harmonic radar," *IEEE Trans. Aerosp. Electron. Syst.*, vol. 50, no. 1, pp. 477–490, Jan. 2014.
[26] J. Owen, S. D. Blunt, K. Gallagher, P. McCormick, C. Allen, and K. Sherbondy, "Nonlinear radar via intermodulation of FM noise waveform pairs," in *Proc. IEEE Radar Conf.*, 2018, pp. 951–956.
[27] J. Owen, C. Mohr, S. D. Blunt, and K. Gallagher, "Nonlinear radar via intermodulation of jointly optimized FM noise waveform pairs," in *Proc. IEEE Radar Conf.*, 2019, pp. 1–6.
[28] R. de Jong, R. van der Zee, and A. Kokkeler, "Analysis of a 1kbps backscatter receiver with up to-80dbm tag-to-tag receive sensitivity," in *Proc. IEEE Int. Conf. RFID*, 2020, pp. 1–8.
[29] A. Lavrenko and J. Cavers, "Two-region model for harmonic radar transponders," *Electron. Lett.*, vol. 56, no. 16, pp. 835–838, 2020.
[30] A. Lavrenko *et al.*, "Autonomous swarm of UAVs for tracking of flying insects with harmonic radar," in *Proc. IEEE 93rd Veh. Technol. Conf.*, 2021, pp. 1–5.
[31] J. Cavers, *Mobile Channel Characteristics*. Cham, Switzerland: Springer, 2006, vol. 555.
[32] K. A. Gallagher, R. M. Narayanan, G. J. Mazzaro, and K. D. Sherbondy, "Linearization of a harmonic radar transmitter by feed-forward filter reflection," in *Proc. Radar Conf.*, 2014, pp. 1363–1368.
[33] A. Lavrenko, G. Woodward, and S. Pawson, "Parasitic harmonic cancellation for reliable tag detection with pulsed harmonic radar," in *Proc. Radar Conf.*, 2019, pp. 1–6.
[34] A. F. Molisch, *Wireless Communications*. Hoboken, NJ, USA: Wiley, 2012, vol. 34.
[35] Skyworks solutions, "SMS7630 series: Surface mount mixer and detector schottky diodes," [Online]. Available: http://www.skyworksinc.com
[36] H. Aumann, E. Kus, B. Cline, and N. W. Emanetoglu, "An asymmetrical dipole tag with optimum harmonic conversion efficiency," in *Proc. Antennas Prop. Soc. Intern. Symp.*, 2012, pp. 1–2.
[37] P. Lawson, J. Godfrey, and A. Lavrenko, "Evaluation of an off-centre fed dipole antenna in passive harmonic radar tags," in *Proc. 4th Australian Microw. Symp.*, 2020, pp. 1–2.
[38] A. Schewelew, "MMANA-GAL: Antenna-analyzing tool based on the moment method," [Online]. Available: http://gal-ana.de/basicmm/en/
[39] R. M. Corless, G. H. Gonnet, D. E. Hare, D. J. Jeffrey, and D. E. Knuth, "On the LambertW function," *Adv. Comput. Math.*, vol. 5, no. 1, pp. 329–359, 1996.

Anastasia Lavrenko (Member, IEEE) received the B.Sc. and M.Sc. degrees in radio systems engineering from Saint Petersburg State Electrotechnical University LETI, Saint Petersburg, Russia, in 2007 and 2009, respectively, and the Ph.D. degree in electrical engineering from the Ilmenau University of Technology, Ilmenau, Germany, in 2018.

From 2018 to 2020, she was a Postdoctoral Fellow with Scion (New Zealand Forest Research Institute) and the Wireless Research Centre, University of Canterbury, Christchurch, New Zealand. She is currently an Assistant Professor with the Radio Systems Group, University of Twente, Enschede, The Netherlands. Her research interests include signal processing for radio systems, microwave sensing, radio localization and positioning, parameter estimation and statistical inference.

James K. Cavers (Life Fellow, IEEE) received the B.A.Sc. degree in engineering physics, and the Ph.D. degree in electrical engineering from The University of British Columbia, Vancouver, BC, Canada, in 1966 and 1970, respectively.

From 1970 to 1979, he was an Assistant Professor, then an Associate Professor, with Carleton University, Ottawa, ON, Canada, after which he was with MacDonald, Dettwiler and Associates in Vancouver. In 1983, he became a Professor with the School of Engineering Science, Simon Fraser University, Burnaby, BC, Canada, then a Professor Emeritus on his retirement in 2008. He is also an Adjunct Professor with the University of Canterbury, Christchurch, New Zealand. He has authored or coauthored more than 130 papers and one book, and holds 12 U.S. patents. His research interests include theory and practice of wireless communication.

Graeme K. Woodward (Senior Member, IEEE) received the B.Sc., B.E., and Ph.D. degrees from The University of Sydney, Camperdown, NSW, Australia, in 1990, 1992, and 1999, respectively.

He has been the Research Leader with the Wireless Research Centre, University of Canterbury, Christchurch, New Zealand, since 2011, and previously the Research Manager of the Telecommunications Research Laboratory, Toshiba Research Europe, contributing to numerous large U.K. and EU projects. His extensive industrial research experience includes pioneering VLSI designs for multi-antenna 3G Packet Access (HSDPA) with Bell Labs Sydney. While holding positions at Agere Systems and LSI Logic, his focus moved to terminal-side algorithms for 3G and 4G (LTE), with an emphasis on low power design. He has authored more than 50 papers and 12 U.S. patents and has served on numerous conference committees.